Directly cooled windings

Conjugate heat transfer assessment of air-cooled hollow conductor

Michael Gabassi

Division of Industrial Electrical Engineering and Automation
Faculty of Engineering, Lund University

Increasing current capacity of machine windings using hollow conductors

Michael Gabassi

Abstract—**The torque capabilities of electrical machines are today limited by magnetic saturation and the ability to transfer thermal loads away from the machine. Using hollow conductors the cooling capabilities are drastically increased allowing for a significant increase in current densities. Results show continuous current density capabilities well in excess of 30 A/mm^2.**

I. Introduction

THE torque capability of an electrical machine is highly dependent on the maximum allowed current through its windings. This maximum current is in turn limited by the heat generated as the current flows through the copper conductors inside the machine. As the copper is heated the insulation between the conductors deteriorates and eventually fails, short circuiting the windings. Modern electrical machines uses water-cooled jackets around the outside of the machine to allow higher currents and thus higher torque. A problem with this method is that the cooling takes place on the outside and not where the heat is generated thus relying heavily on good thermal connection to the inside the machine. A solution to this problem widely used in larger electrical machines is found in the use of a hollow conductors where a cooling fluid passes through interior channels. This cooling method allows for direct cooling of the heat source with a significant increase in current capabilities. The work done as part of this master thesis attempts therefore to predict the cooling performance of hollow conductors intended for use in a smaller electrical machine.

II. Components examined

Four different components have been examined using compressed air as cooling fluid. The two leftmost components shown in 1 represents the simplest possible case and was used to gain a good understanding of the general physics. Once this was achieved a progression towards a components similar to an actual electrical machine winding were used, shown in the middle column.
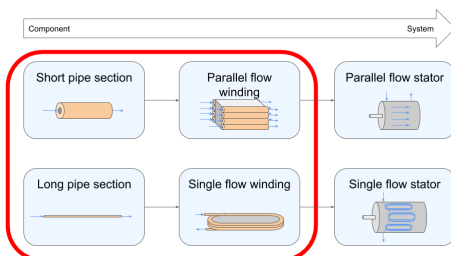

Fig. 1. The examined components and their intended implementation

By measuring the current flowing through the copper and the inlet pressure of the airflow a relationship between the power needed to cool the machine and the maximum possible current density is obtained. These results can then be used to assess which method is the best and what levels of current density can be achieved.

III. Results

The measured current capabilities from experiments made on the parallel flow winding, see figure 1, is shown below. As a general reference the uncooled hollow conductor will overheat at a current density of 12-15A/mm^2, with temperatures rising above 180°C.
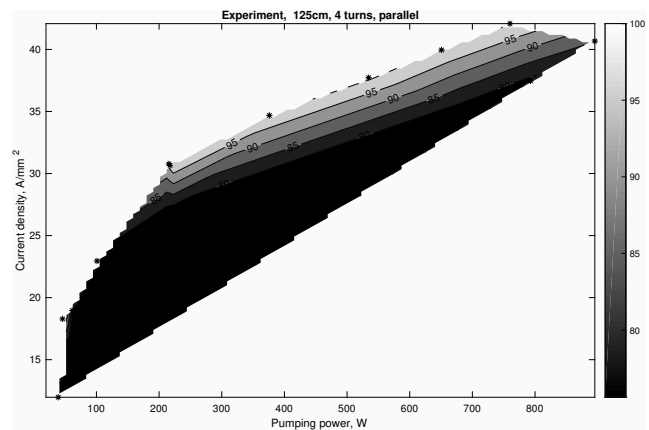

Fig. 2. Current capabilities of the air-cooled parallel flow winding, the top

By flowing compressed air through the parallel flow winding it is possible to more than triple the current flowing through it while still keeping a maximum temperature below 100°C. This is achieved using a theoretical pumping power of approximately 100W per cooling channel. The results also show that a significant increase in current capabilities can be achieved already at 10W per cooling channel if a higher maximum temperature is allowed.

IV. Conclusion

Experiments using compressed air show great potential for direct cooled windings: the use of hollow conductors allows for a significant increase in current capabilities, thereby opening up possibilities for a new generation of electrical machine cooling.

Abstract

The torque capabilities of electrical machines are today limited by magnetic saturation and the ability to transfer thermal loads away from the machine. A solution to thermal management in power turbo-generators involves hollow conductors allowing direct cooling of the heat source thus increasing the power density significantly. The work done in this master thesis investigates the possibilities of implementing such cooling techniques in smaller electrical machines and predicts the current capabilities of directly cooled conductors. Experiments have been made on hollow conductors using compressed air as cooling fluid and mathematical models are used to predict the capabilities of using oil as coolant. Results show current density capabilities in excess of $30\mathrm{A/mm}^2$. Results from experiments are compared to finite element studies and mathematical models to assess validity.

Preface

This master thesis project has been a part of the Supercool project conducted at the Department of Industrial Electrical Engineering and Automation (IEA). The aim of the project is to assess cooling alternatives for electrical machines and this master thesis focuses on the cooling performance of hollow conductors using compressed air as coolant. The work was carried out at one of the IEA's labs in Lund.

Acknowledgements

Contents

1 Introduction

1.1 Background

As the automotive industry continues its progression towards alternative drive systems the role of electrical machines becomes more and more significant. Similar trends are observed in the aeronautical industry where the demand for onboard electric power is continuously increasing. One of the electrical machines main limiting factors is the thermal capabilities of the winding and its insulation. In larger generators directly cooled winding using hollow conductors have been used in over 60 years allowing much greater power ratings for a given machine size [1]. These machines allow efficient cooling d irectly at the heat source thus greatly increasing the current capabilities of the conductors.

1.2 Research aim

The aim of this project is to investigate the cooling capabilities of hollow conductors using air as a cooling fluid. The current density capabilities of hollow conductors will be assessed through experiments, mathematical models and FE analysis. The knowledge gained will guide future research on the subject and present related challenges and opportunities.

1.3 Research limits

The project will only address the cooling of the hollow copper conductors described in section 5. No consideration will be taken to the power needed in compression of the air used and the heat generation involved.

1.4 Outline

The general structure of the report is according to the IMRAD format. A short description of each section is shown below.

2 Losses in electrical systems

This section describes how the heat is generated inside the conductor using a A 50Hz AC current.

3 Fluid Mechanics

When studying the cooling performance of a fluid moving through a pipe it is important to fully understand and to be able to predict the underlying fluid mechanics. This section describes the relevant theory and the different characteristics of fluid flow through a narrow channel. In order to do this some basic fluid terminology is introduced.

4 Heat Transfer

This section describes the relevant heat transfer physics of this work. Efficiently combining heat transfers in solids and fluids is an important part of efficient cooling performance where forced convection plays a key role.

5 Components examined

This section describes the four components examined and how they are related to each other.

6 Design of experiments

To understand the performance and cooling capabilities of a DCMW three different methods of research were chosen. This section briefly describes the initial literature study and each of the three different methods used to analyze each of the four components.

7 FE Analysis

When deciding what software to use in the finite element study two options were considered, Comsol Multiphysics and Autodesk CFD. After a short study of the capabilities of the two Comsol was chosen, mainly due to the flexibility of the software and its multiphysics capabilities. This section describes some underlying theory and how the simulations were set up.

8 Mathematical model

Another approach to estimating the cooling performance of a hollow conductor is through the analytical and empirical relations mentioned in section 3 and 4. These relations are used to create a mathematical model of each component in Matlab. This section describes the general working method of the model and some of the assumptions made.

9 Experiment setup

This section describes the setup used for each of the four components and the measurement equipment used.

10 Results

The results from each of the methods used to examine each component is presented first in this section. The last part of this section contains a few interesting measurements described in the following section.

11 Discussion

The results are discussed in the order presented in the previous section. The accuracy of the measurements made is discussed together with conclusions based on the findings. The three methods used are also compared and thoughts regarding any discrepancies between these are presented.

12 Summary

The results are condensed into a short summary describing the possibilities of direclty cooled windings.

13 Future studies

The work done during this master thesis project is only a scratch on the surface of the directly cooled winding possibilities. Two different future paths are presented together with some predictions of cooling performance of an alternative cooling fluid.

2 Losses in electrical systems

This section describes how the heat is generated inside the conductor using a A 50Hz AC current.

2.1 DC Systems

The power delivered to a DC electrical system is equal to the voltage across the system multiplied by the current flowing through it:

$$P = U * I \tag{1}$$

According to ohms law, the voltage across the system is the product of the current and the system's resistance:

$$U = R * I \tag{2}$$

For the system analyzed as part of this project the resistance of the copper winding is calculated as:

$$R = r * \frac{L}{A} \tag{3}$$

where r is the coppers resistivity, in this work linearized by the following relation:

$$r = r_{ref} * \alpha * (T - T_{ref}) \tag{4}$$

2.2 AC losses

As long as the current and voltage in an AC system are in phase the losses in the systems can be derived using the same relations as in the DC case by substituting the current and voltages to their RMS equivalents. AC losses for inductive circuits will not be covered in this work as all loads are assumed purely resistive.

3 Fluid Mechanics

When studying the cooling performance of a fluid moving through a pipe it is important to fully understand and to be able to predict the underlying fluid mechanics. This section describes the relevant theory and the different characteristics of fluid flow through a narrow channel. In order to do this some basic fluid terminology is introduced. This terminology is used to divide the fluid's characteristics into the different categories presented in figure 1 and 2 below.
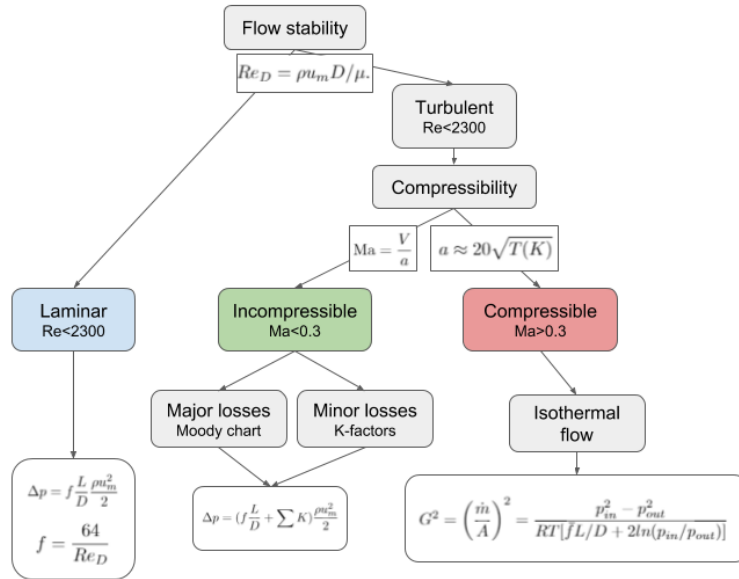
Figure 1: Flow categorization
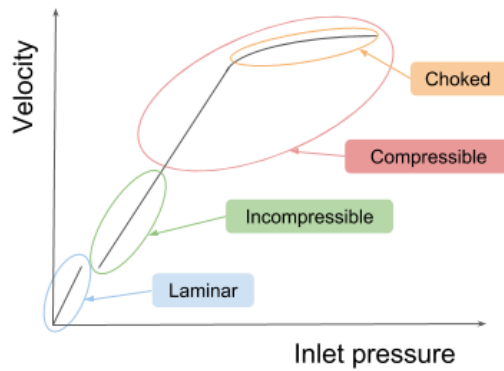

Figure 2: Flow categorization

3.1 Reynolds Number

A simple means of describing any fluid flow is through the use of the dimensionless parameter Reynolds number

$$\mathrm{Re} = \frac{\rho V L}{\mu} \tag{5}$$

where V and L are the characteristic velocity and length of the flow, ρ density and μ is the dynamic viscosity. When studying flow through pipes, the diameter

represents the characteristic length. Reynolds analogy states that the flow field around or inside geometrically similar bodies are identical if the Re number is equal and the boundary conditions are the same. The Reynolds number (Re) can be regarded as the level of turbulence in a flow where a low Re implies a slow moving, creeping flow (think of thick oil slowly flowing along a plate) and a high Re implies a random, turbulent flow with a high level of vorticity (think of compressed air through a small nozzle).[4]

3.2   Mach number

As the velocity of the air in a system increases it will eventually flow faster than the local speed of sound. The relation between the air velocity and the local speed of sound is called the Mach number, defined as:

$$\text{Ma} = \frac{V}{a} \tag{6}$$

where V is the velocity of the fluid and a is the local speed of sound for air, approximated as:

$$a \approx 20\sqrt{T(K)} \tag{7}$$

This approximation is valid whenever considering air as a perfect gas, which holds well for dry air at the intended temperatures[4]. The Mach number is an important part of understanding any system as the flows characteristic changes considerably when reaching the transonic and supersonic ranges.[4]

3.3   Laminar flow

A laminar flow is a predictable flow with little or no vorticity where analytical relations for the flows characteristics are available. Generally a flow is considered Laminar when Re<2300. The actual transition level depends on other factors as well however Reynolds is commonly regarded as the main parameter. As the fluid enters the pipe the initial velocity profile will not be fully developed. At the inlet the fluid will gradually develop into its fully developed state and the length required for this is called entrance length. Once the flow has reached its fully developed profile the fluid nearest to the wall will be stationary, this is known as the no-slip condition, with a gradual increase in velocity towards the center of the pipe [2]. A typical velocity profile for fully developed laminar flow is shown in figure 3 together with a schematic of the flow development at the pipe entrance.
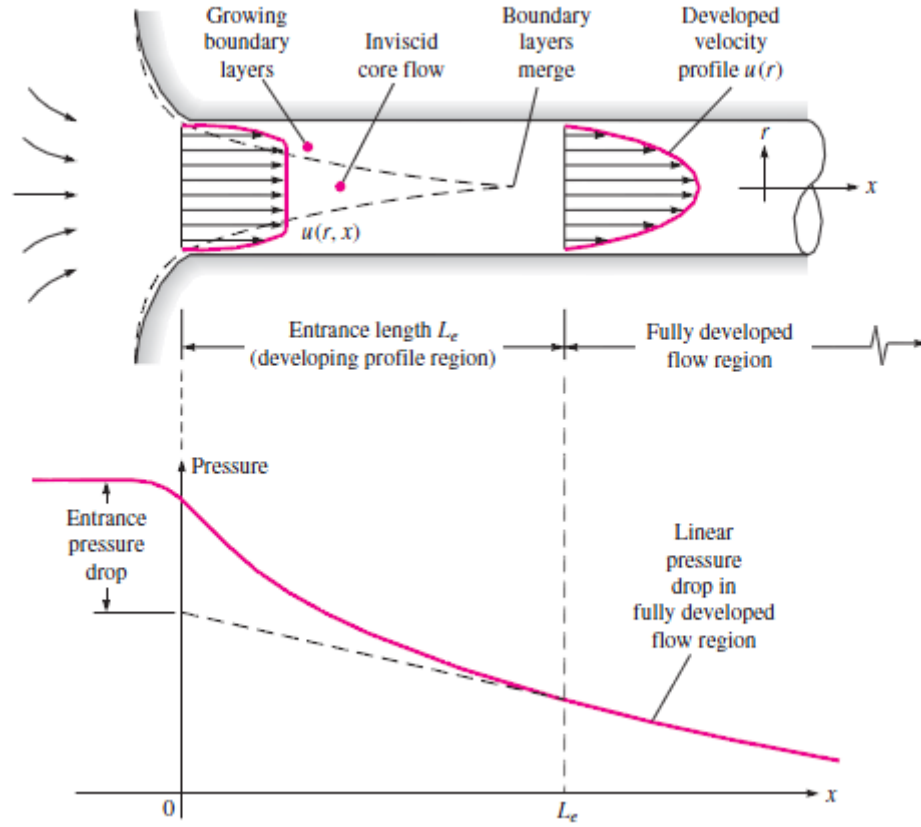
Figure 3: Entrance length and typical velocity profile for laminar flow, taken from [4]

The pressure drop across a set pipe length for a given average velocity can be calculated as:

$$\Delta p = f \frac{L}{D} \frac{\rho u_m^2}{2} \tag{8}$$

where ρ is the fluid density and f is the friction factor. For a circular pipe the friction factor can be expressed as:

$$f = \frac{64}{Re_D} \tag{9}$$

where $Re_D = \rho u_m D / \mu$.

Given these expressions the flow can be considered laminar until, as previously mentioned, Re_D reaches 2300 which for a 2mm*1000mm pipe equates to an average velocity of 17.5 m/s at a pressure drop of 25 mBar. For the intended application it does not appear practical to consider laminar flow when using air as cooling fluid as the resulting heat transfer coefficient would be too low for

any cooling application. If however a more viscous fluid (such as water or oil) is used a laminar flow may very well provide the needed cooling performance. [4]

3.4 Turbulent flow

As opposed to laminar flow, the turbulent flow is characterized by high levels of fluctuations in vorticity, randomness as well as high levels of diffusion and dissipation [3]. Due to the increased impulse exchange of the fluid the velocity profile will be more uniform towards the middle with a thinner region of slower air along the inner surfaces of the pipe (no-slip condition still applies). A comparison between a laminar and turbulent flow profile is shown in figure 4
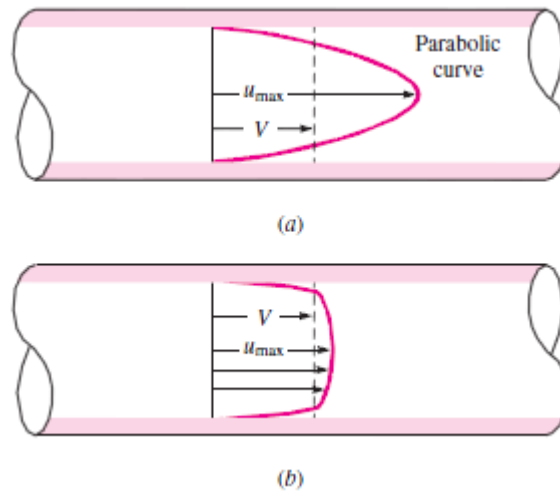

Figure 4: Typical velocity profile for a) laminar flow and b) turbulent flow, taken from [4]

3.5 Incompressible flow

Due to the fact that air is a compressible fluid care must be taken when working with high-velocity flows to ensure that any compressibility effects are considered. Such effects are theoretically present at any speed but it is common to consider a flow with a maximum velocity below Mach 0.3 as incompressible, thus neglecting any density variations. This simplification allows for the use of the *Bernoulli equation* [4]:

$$\frac{p_1}{\rho} + \frac{V_1^2}{2} = \frac{p_2}{\rho} + \frac{V_2^2}{2} \tag{10}$$

The requirement for speeds lower than Mach 0.3 means that for a flow in room temperature, the limiting velocity is roughly 100 m/s. Depending on the length of the pipe, this speed will be reached at different pressure differentials thus requiring attention as to not exceed this value in any calculations based on the incompressibility assumption.

Pressure drop

Deriving the pressure drop for a given flow velocity (or vice versa) is similar to the laminar case with the addition of minor losses which factors in losses due to geometry of the system components (valves, inlets and outlets).

Major losses

Major losses describes the pressure drop due to friction along the length of the pipe. The only difference of these losses as compared to the laminar case in (4) is that the friction factor f is obtained from a Moody chart shown in figure 5. In the chart two regions are highlighted, the darker lines represents the corresponding friction factors for a new, unused pipe and the lighter lines are values for a used pipe.
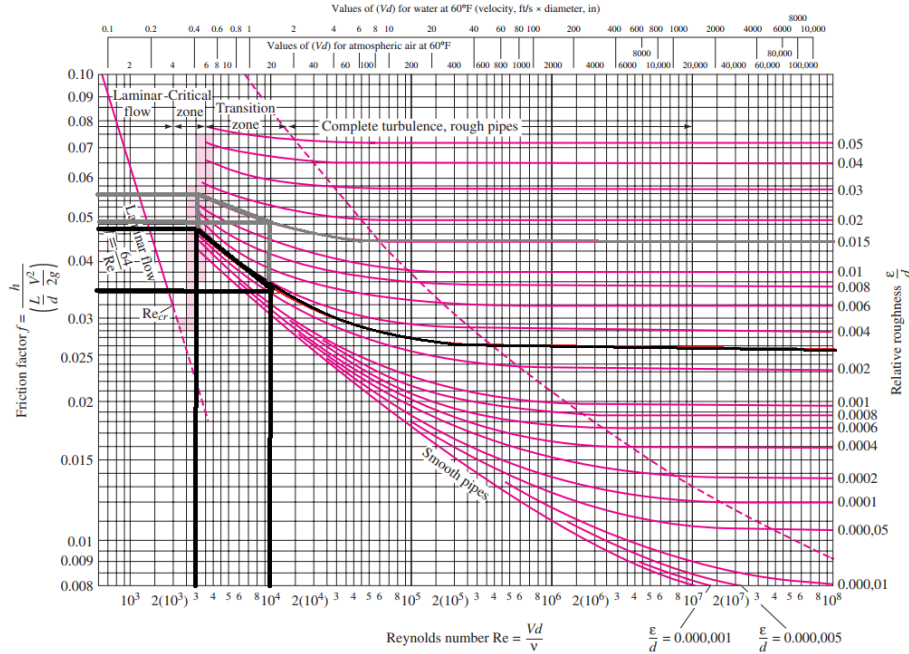

Figure 5: The Moody diagram with working area for 2mm*200mm pipe highlighted [4]

Minor losses

Once the pressure drop due to friction losses has been determined any components that may affect the flow should be included in the calculations. For the set up used in this thesis, the system consists of one inlet and one outlet where the corresponding K-factors are obtained through empirical results. These K-factors are added to (4) as:

$$\Delta p = (f\frac{L}{D} + \sum K)\frac{\rho u_m^2}{2} \tag{11}$$

which will give the total pressure drop for the system.

3.6 Compressible flow

All of the previous sections have been concerned with low speed, or incompressible flow and as the speed of the airflow increases the density of the air can no longer be considered constant. When working with gases a pressure ratio of 2:1 is likely to cause sonic flow [4]. As a result the previously mentioned equations for determining the pressure drop can no longer be used and new methods of determining the flows characteristics must be used. Two important effects of compressibility is the appearance of shock waves, which are almost instantaneous changes in fluid properties along the flow path and choking which is a term to describe the flow rate limit imposed on a flow at sonic speeds. Although available theory on shock waves and supersonic flow is vast this thesis will only consider subsonic or sonic flow in ducts (pipes) with a constant cross section.

Isothermal flow

If an assumption is made that no heat is added or removed from the flow, the relationship between pressure and mass flow can be described as:

$$G^2 = \left(\frac{\dot{m}}{A}\right)^2 = \frac{p_{in}^2 - p_{out}^2}{RT[\bar{f}L/D + 2ln(p_{in}/p_{out})]} \tag{12}$$

This relationship allows for a straight forward calculation of the velocity and volume flow as long as the velocity is subsonic. This requires that any results obtained from the above equation must be checked for choking by examining the mach number at the outlet of the pipe. As the mass flow is constant along the pipe length the outlet velocity can be obtained by the following relation:

$$\dot{m} = \rho\dot{V} = \frac{p_{out}v_{out}A}{RT} \implies v_{out} = \frac{\dot{m}RT}{p_{out}A} \tag{13}$$

Where $R = 287$ for air and A is the cross section area of the pipe. The resulting outlet Mach number should for isothermal flow be less than $1/k^{1/2}$ to ensure that the flow is not choked.

3.7 Choked flow

As the pressure differential between inlet and outlet increases, at some point the exit speed of the fluid will reach $M = 1/k^{1/2} = 0.845$. Once this occurs, the flow is said to be choked and as a consequence the mass flow through the pipe cannot be increased any further through a reduction of the outlet pressure. The only way to increase the mass flow beyond this point is through an increase in inlet pressure as this will increase the density of the fluid at the inlet. The maximum entrance Mach number can be derived using the following equation:

$$\frac{\bar{f}L^*}{D} = \frac{1 - \text{Ma}^2}{k\,\text{Ma}^2} + \frac{k+1}{2k}\ln\frac{(k+1)\text{Ma}^2}{2 + (k-1)\text{Ma}^2} \tag{14}$$

where Ma is the entrance mach number resulting in a choked flow, L^* the length of the pipe, D is the diameter and $\bar{f}$ is the average friction number. From a cooling perspective this does not mean that the cooling performance is choked as the following section will show that the heat transfer coefficient is a function of Reynolds number which continues to increase with an increasing mass flow.

4 Heat Transfer

4.1 Heat conduction

Whenever a temperature difference exists within an object a transfer of heat will occur from the warmer region to the colder region. The intensity of this flow is defined as the materials thermal conductivity and is commonly denoted by λ. The transfer of heat is called heat flux and is written as:

$$q = -\lambda \frac{\delta t}{\delta n} \tag{15}$$

4.2 Heat convection

If a temperature difference is present between a surface and a surrounding fluid convection will occur where the heat will flow from the warmer region to the colder. The convective heat flux is similar to the conductive apart from the temperature gradient now defined as the difference between the fluid temperature, t_f, and the wall temperature t_w:

$$\frac{\dot{Q}}{A} = q = \alpha(t_f - t_w) \tag{16}$$

where A is the surface area and α is the heat transfer coefficient. The heat transfer coefficient plays a central role whenever studying cooling performance. Unfortunately it is difficult to determine as it is only known for the cases of a constant surface temperature or a constant wall flux, neither of which are rarely true in any application. The rest of the theory on heat transfer will therefore cover the different methods of determining the heat transfer coefficient.[2]

Laminar vs turbulent

From a cooling perspective a turbulent flow is desirable as the increased impulse exchange allows for a more even heat distribution across the pipes cross-section. A laminar flow will only allow a heat exchange along the boundary layer meaning that less of the available volume flow is utilized. [4]

4.3 Prandtl number

The Prandtl number is the relation between a fluids dissipative properties and its conductive properties, defined as:

$$\text{Pr} = \frac{\mu c_p}{k} \tag{17}$$

where μ is the dynamic viscosity, c_p the specific heat and k the thermal conductivity of the fluid. The Prandtl number can be seen as a fluids heat transfer capabilities for a given flow situation where high Pr numbers will mean less heat transfers than low Pr numbers. [2]

4.4 Nusselt number

Similar to Reynolds analogy the Nusselt number describes the properties of a temperature field around or inside geometrically similar bodies. For a steady-state flow, the Nusselt number is a function of both the Reynolds number and the rules of similarity is formulated so that the temperature field around or inside similar bodies are identical if the Nusselt number and boundary conditions are the same. The Nusselt number is used to calculate the heat transfer coefficient as:

$$\text{Nu} = \frac{\alpha L}{\lambda} \tag{18}$$

where α is the heat transfer coefficient mentioned in (16), L is the characteristic length (L=D for flow in pipes), and λ is the thermal conductivity of the fluid.[2]

4.5 Determining the heat transfer coefficient

Laminar flow

As the intended cooling scenario assumes a uniform heat flux along the boundary the following relation for the Nusselt number can be used to determine the heat transfer coefficient for a laminar flow scenario:

$$\overline{\text{Nu}}_D = \begin{cases} 1.953 \left(\dfrac{1}{\text{Re}_D Pr} \dfrac{x}{D} \right)^{-1/3} & \text{if } \frac{x/D}{\text{Re}_D \text{Pr}} < 0.03. \\ 4.364 + \dfrac{0.0722}{x/D} \text{Re}_D \text{Pr} & \text{if } \frac{x/D}{\text{Re}_D \text{Pr}} > 0.03. \end{cases} \tag{19}$$

where x is the length of the pipe. This Nusselt number is an average for the specified length of pipe including any entrance effects.[2]

Turbulent flow

A turbulent flow is characterized by high levels of vorticity and mixing of the fluid. From a convective heat transfer perspective this is beneficial as more of the fluid will be able to absorb or transfer heat to or from a surface. Today there is no exact solution to the navier stokes equations for turbulent flow meaning that a study of heat transfer in turbulent flow relies heavily on empirical relations and dimensional analysis. Many of these empirical relations use another dimensionless number called the Stanton number, defined as:

$$\text{St} = \frac{\text{Nu}}{\text{RePr}} \tag{20}$$

Once the Stanton number is calculated and the Reynolds and Prandtl number is known, the heat transfer coefficient can be obtained using the relation given in (18). One way of determining the St is through the following relation developed by Theodore von Kármán:

$$\text{St} = \frac{f/8}{1 + 5\sqrt{f/8} \left\{ (\text{Pr} - 1) + ln[(5\text{Pr} + 1)/6] \right\}} \tag{21}$$

4.6 Specific heat capacity

The specific heat capacity of a material describes how much energy is needed to achieve a certain temperature difference. For a fluid flowing through a pipe, the temperature rise from inlet to outlet due to the heat load can be written as:

$$Q = \dot{m} * c_p * (T_{out} - T_{in}) \tag{22}$$

where Q is the heat load and c_p is the specific heat capacity of the fluid.

5 Components examined

An overview of the components is shown in figure 6 with the components studied in this work encircled.
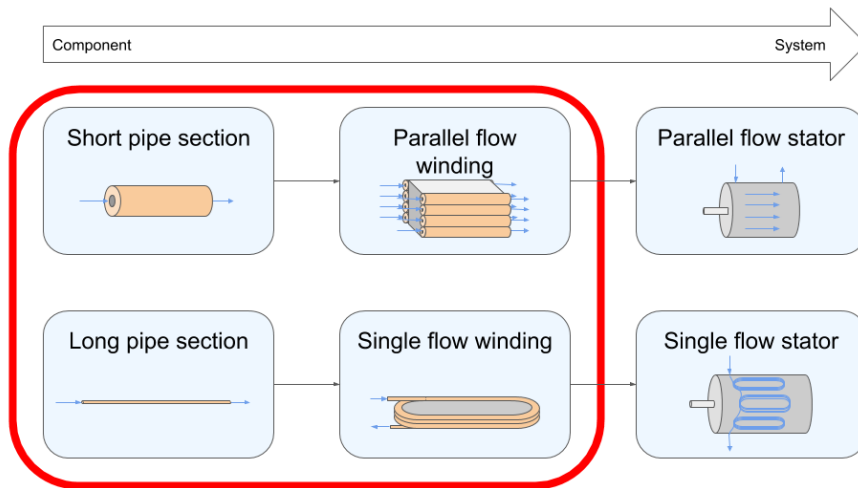
Figure 6: Overview of the components studied

5.1 200mm copper pipe

In order to understand the capabilities of a directly cooled winding a simple 200mm copper pipe is chosen as the initial component to examine, see figure 7. The component has an outer diameter of 4mm and an inner diameter of 2mm and is heated uniformly by resistive heating. The conductor is cooled through fluid flowing through its central cavity.
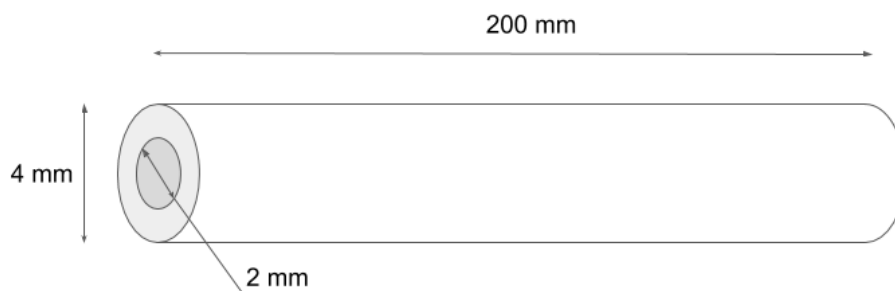
Figure 7: The first component examined, a 200mm copper pipe

5.2   880mm hollow conductor

The second component, a 880mm hollow conductor section, is analyzed using the same methods as the previous and the results are compared. This conductor has a rectangular cross section with dimensions shown in figure 8.
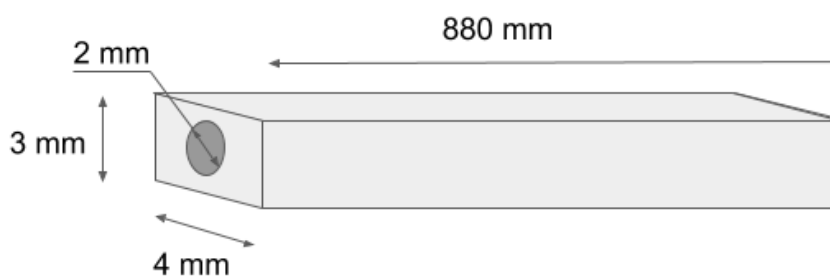
Figure 8: The second component examined, a 880mm hollow copper conductor

5.3   4-turn wound hollow conductor

As the understanding of the physics of the components illustrated above is improved, the next step is to examine a component more similar to an actual electrical machine winding. This is respresented by a 1250mm, 4-turn winding of the hollow rectangular conductor illustrated in figure 8. An image of the winding used in the experiments made is shown in figure 9. The winding is mounted inside a glass-fiber holder representing a stator section of an electrical machine.
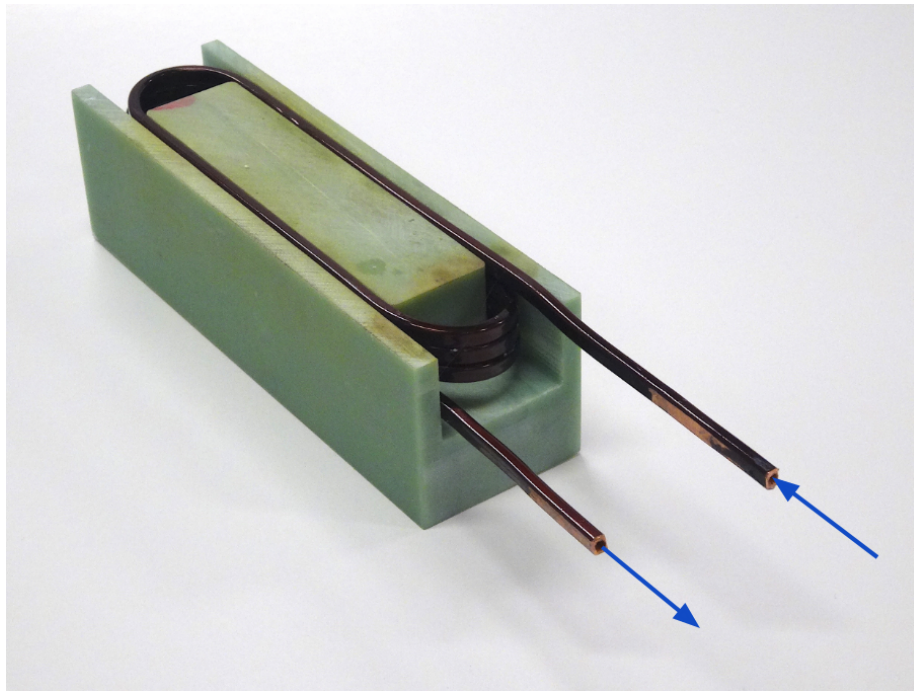
Figure 9: The 4-turn hollow conductor mounted inside a fiberglass bobbin in the single flow configuration.

Single flow

The 4-turn conductor is tested in two configurations where in the first setup the cooling is led through the entire conductors length as shown in figure 9. Besides the bobbin and the fact that the conductor is wound, from a heat transfer perspective this configuration shares many similarities to the 880mm hollow conductor.

Parallel flow

The final configuration is the same parts used in the preious section but this time with 8 holes drilled on either side of the winding. In this configuration the cooling fluid flows through 8 parallel channels from one side of the bobbin to the other, see figure 10. Apart from the surrounding materials this component is thermally similar to the 200mm component previously mentioned.
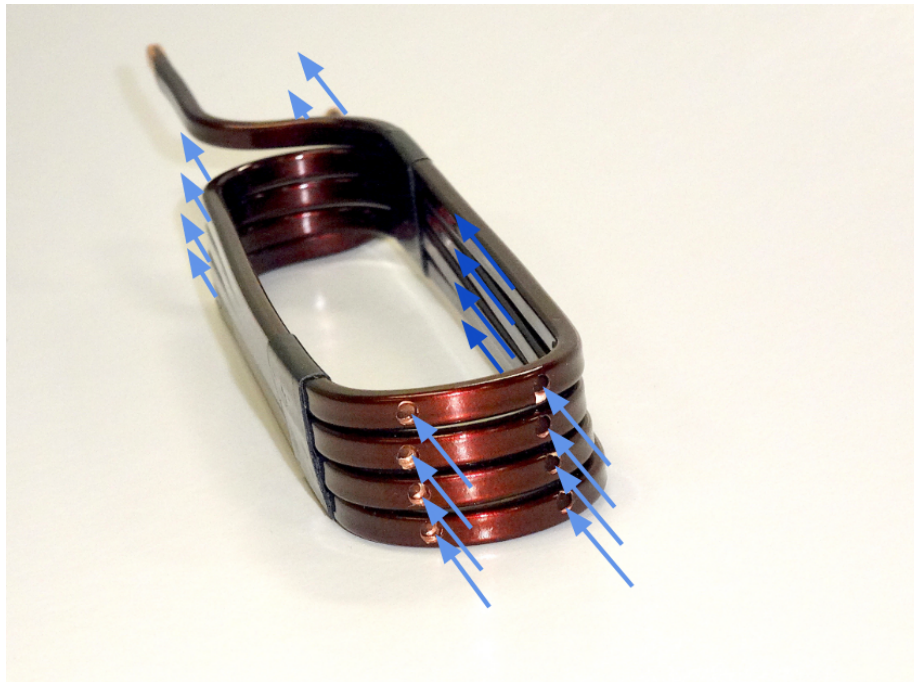
Figure 10: The 4-turn hollow conductor mounted inside a fiberglass bobbin with the parallel flow configuration.

6 Design of experiments
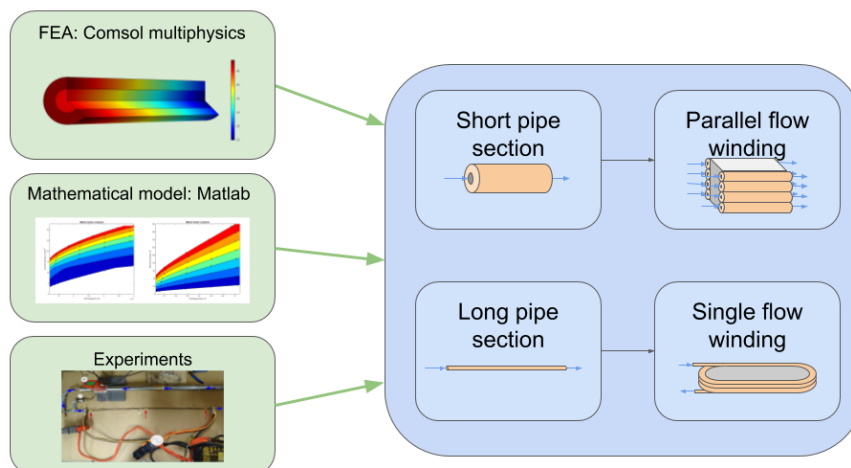
Figure 11: Overview of the three methods applied to the four components

To understand the performance and cooling capabilities of a DCMW three different methods of research were chosen. Before any investigative research was initiated a literature study was made on the subject of heat transfer, using mainly the heat transfer course literature *Introduction to Heat Transfer* written by Bengt Sundén. In order to gain as much knowledge as possible and to some extent validate any intermediate results three different approaches are used, see figure 11. The first approach is a finite element analysis followed by a mathematical model using the empirical relations mentioned in section 3 and 4. The final approach is an experimental set up in the IEA lab. Throughout the process updates are made continuously to the three methods of study as more knowledge is gained.

6.1 Hot spot temperature

If the heat load does not have any other paths than the cooling fluid the maximum temperature of the conductor will occur at the exit of the flow as this is where the fluid reaches its maximum temperature. Thus the studies are mostly concerned with calculating the copper temperature at the outlet of the flow which will also be the temperature presented in the results section.

7 FE Analysis

When deciding what software to use in the finite element study two options were considered, Comsol Multiphysics and Autodesk CFD. After a short study of the capabilities of the two Comsol was chosen, mainly due to the flexibility of the software and its multiphysics capabilities.

7.1 Comsol Multiphysics

The Comsol Multihpysics suite offer a wide range of modules for multiphysics modelling and the main modules used in this work are:

- Heat transfer Module

- Laminar Flow Module

- Turbulent flow Module

Studies were also made on the usability of two additional modules:

- Pipe Flow Module

- AC/DC Module

7.2 2D Axisymmetric

Due to the simple geometry of the analyzed components a two-dimensional axisymmetric study is made on each component. This greatly reduces required computing power and computing times thus allowing more studies to be made on each component.

880mm hollow conductor

The 880mm hollow conductor is simplified to a equivalet circular cross section with equal areas as the actual component.

4-turn component simplification

The 4-turn single flow component will be modelled using a straight pipe of the same length and an outer diameter corresponding to the same volume. The 4-turn parallel flow is not modelled as it essentially consists of eight 200mm copper tubes in parallel.

7.3 Heat Transfer Module

The Heat transfer module is a simple straight forward module allowing the user to input a set of heat boundary conditions to a predefined geometry together with relevant material properties.

7.4 Turbulence models

Due to the lack of exact solutions to turbulent flow Comsol uses a number of different formulations to solve different flow problems. Each of these formulations are designed for different problems and this work will only use the Algebraic yPlus model with its accompanying wall functions. The chosen turbulence model is the most robust and least computationally intensive models available and generally the least accurate. However this model is according to Comsol expected to provide a good estimation of the cooling performance. [5]

Wall functions

When modelling turbulent flow comsol uses wall functions to simplify simulations by approximating the fluid flow along the boundaries. A wall function assumes that the flow closest to the boundaries are laminar and thus analytical solutions can be used to calculate the flow. The accuracy of this simplification can be verified through the parameter called "wall resolution viscous units".
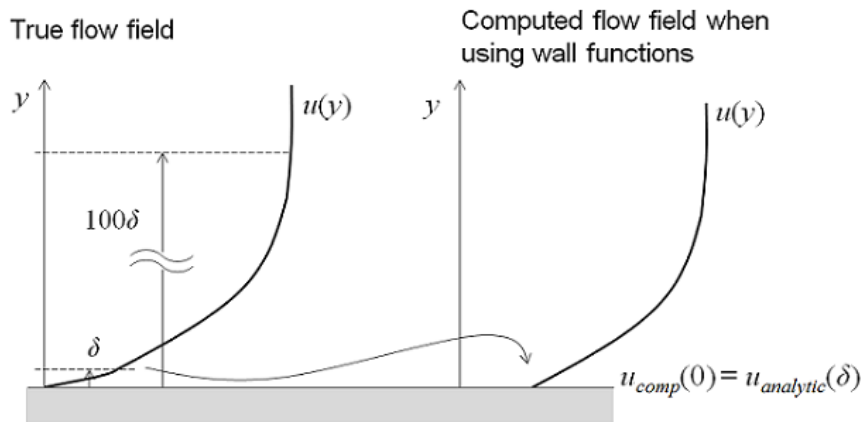
Figure 12: Description of Comsol's wall functions, taken from [5]

7.5 Boundary conditions

The boundary conditions for the FEA analysis are shown in figure 13. The inlet temperature is set to 20°C and the outlet pressure is set to 0 Pa. The distributed heat source in the copper is varied as well as the inlet pressure.
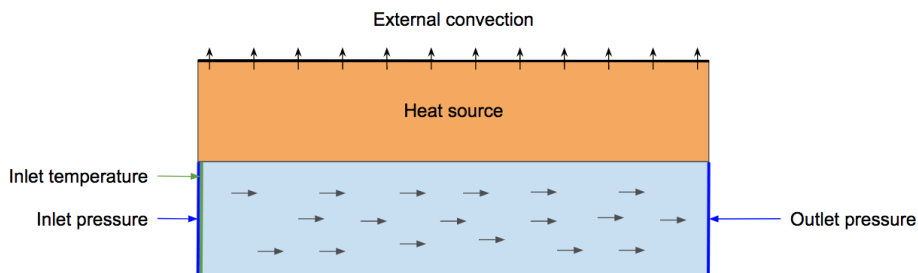

Figure 13: Boundary conditions used during FE simulations.

7.6 Mesh

The built-in meshing control of comsol is effective at generating a good mesh for the simple geometry of this work. Using the automated meshing also allows for the software to adapt the boundary layers to the wall functions, reducing simulation times. A typical mesh used is shown in figure 14.
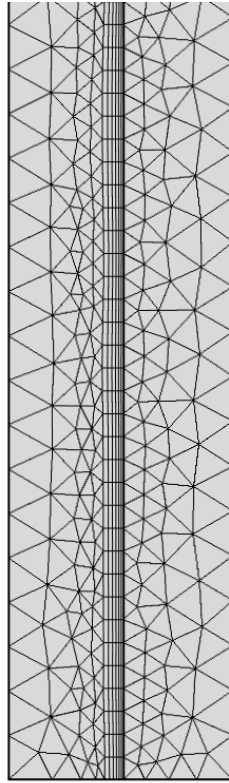
Figure 14: Mesh used in FE simulations

7.7 Pipe Flow module

The Pipe Flow module included in the Comsol Multiphysics suite is used in simulations of fluid flow, heat transfer, hydraulic transients and acoustics in pipe and channel networks. The advantage of this module is that a pipe and its fluid flow is modelled as a one-dimensional line where the internal flow and boundary heat transfer is solved using relevant equations and correlations instead of a FE analysis. This reduces calculations times drastically and consequently allows for much greater complexity in geometries. When using this module in heat transfer simulations the boundary heat flux can either be calculated automatically by comsol using Nusselt number correlations similar to those mentioned in previous sections, or specified manually. Because the pipes are modelled as lines and not three-dimensional some modifications must be made to the model in order to accurately represent the actual model. Because the examined conductors have a typical outer diameter of 2mm a dummy material has to be added in the void around the one-dimensional line. This dummy material is constructed in comsol with an infinite thermal conductivity in the radial direction of the pipe thereby projecting the results of the one-dimensional pipe onto the inner surfaces of the actual pipe. An illustration of a conductor section with the one-dimensional line representing a pipe is shown in figure 15.
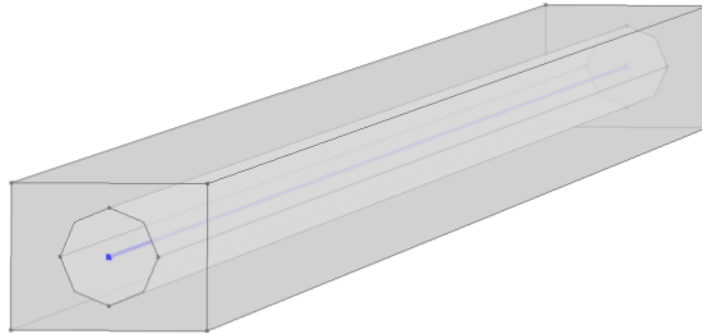
Figure 15: Illustration of a one-dimensional pipe (blue line) used in comsol's Pipe Flow Module

7.8 Post-processing

Once simulations have been made the resulting copper temperatures and flow data are transferred to matlab where the inlet pressure is used to calculate the pumping power using the models described in figure 16.

8 Mathematical Model

Another approach to estimating the cooling performance of a hollow conductor is through the analytical and empirical relations mentioned in section 3 and 4. These relations are used to create a mathematical model of each component in Matlab. An coarse overview of the model for turbulent air flow is shown in figure 16. No studies were made on laminar air flow due to the poor cooling performance at the associated Reynolds numbers.
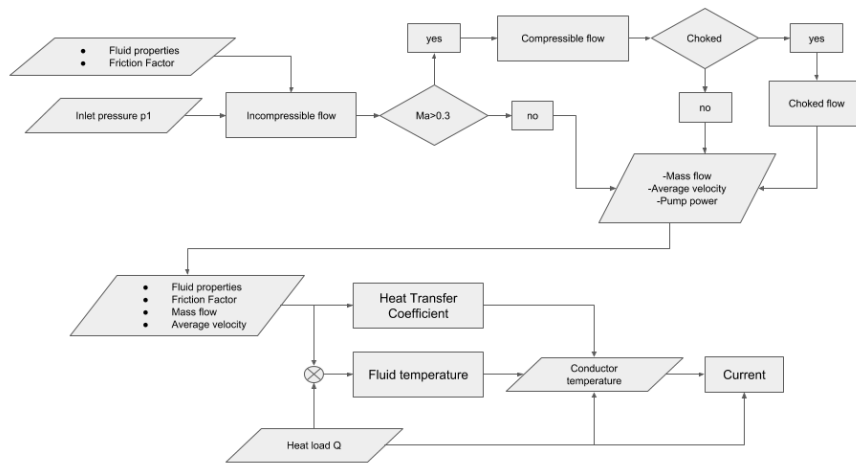
Figure 16: Overview of the model written in Matlab for turbulent air flow, the top half covers the fluid mechanics and the bottom half covers the heat transfer.

8.1 Fluid mechanics

The model is coarsely divided up in two steps where the first step is determining the flow given a certain inlet pressure, friction coefficient and pipe geometry. Here, the equations presented in section 3 are used according to the flow chart in figure 16 and the resulting mass flow and average velocity is then fed to the next section of the model.

8.2 Heat transfer

Once the flow is determined the heat transfer coefficient can be calculated using the equations described in section 4.5. Simultaneously, the outlet temperature of the fluid is calculated using the give mass flow, specific heat capacity and inlet fluid temperature according to (22). Once the fluid temperature and heat transfer coefficient is known the copper temperature can be calculated using equation 16 where the heat load q is obtained from the set heat load Q. The last step of the model is to calculate what current is needed at the given average copper temperature to generate the set heat load.

8.3 External convection

The model presented in figure 16 assumes that the entire generated heat load is absorbed by the fluid flowing internally which is perhaps not entirely correct. Using data obtained from the experiments made the model is updated to account for any external convection that may be present. The external heat transfer coefficient is obtained by measuring the difference between the exterior surface temperature and the ambient temperature. A flow chart of the updated model is presented in figure 17.
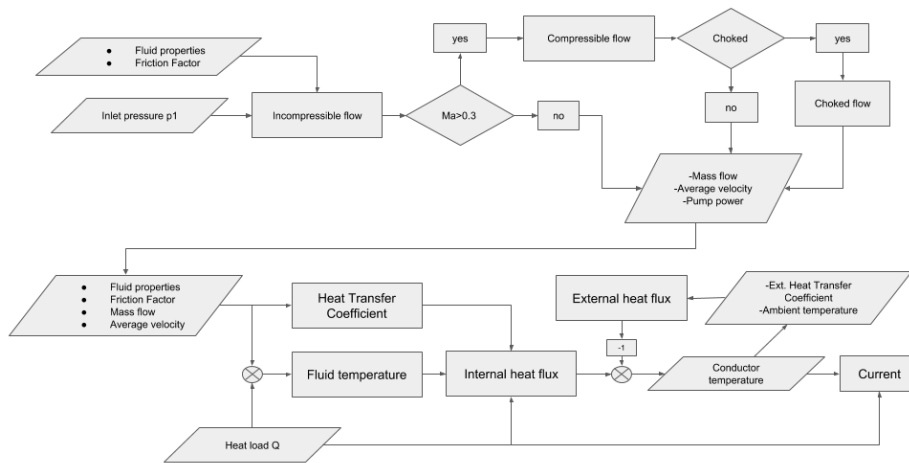
Figure 17: Overview of the updated model written in Matlab for turbulent air flow, including convection to ambience.

9   Experiment setup

For the various studies different variations of the setup illustrated in figure 18 is used. The illustration does however give a good overview of the general layout of the experiments.
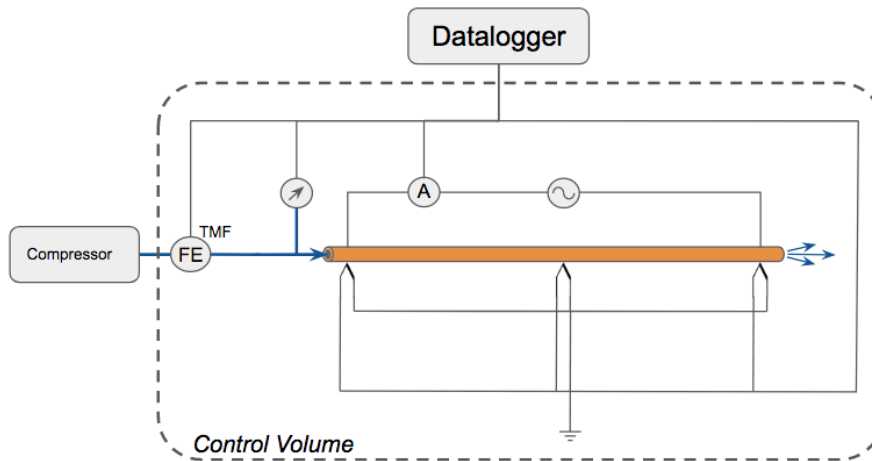

Figure 18: Illustration of one of the experimental setups used.

9.1 200mm Copper Tube

The first experiment is made using the 200mm copper tube described in section 5.1. Figure 19 shows the setup with the BenchLink interface running. In order to reduce external heat transfer the pipe is embedded in a foam casing.
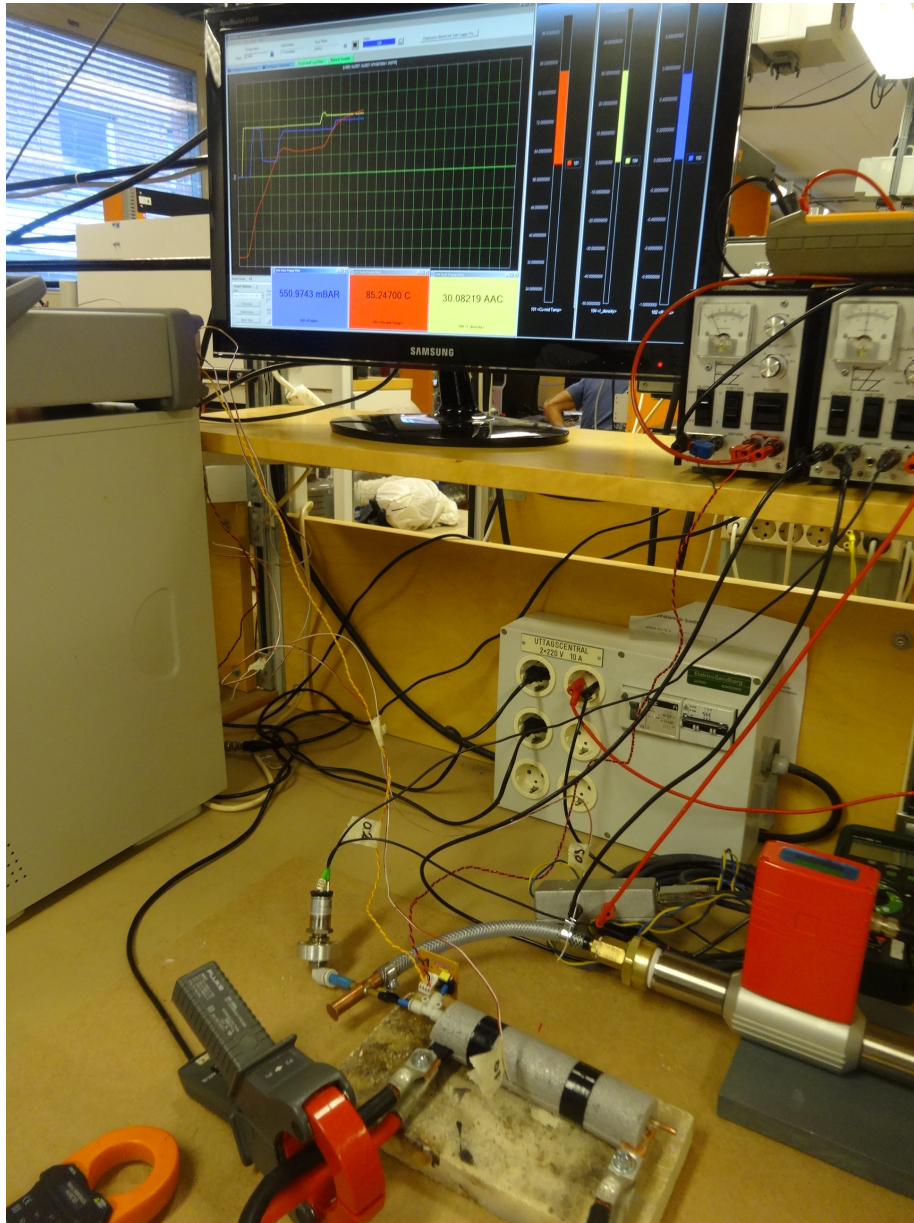
Figure 19: The setup used for the 200mm copper pipe.

9.2   880mm Hollow Conductor

The experiment on the second component described in section 5.2 is shown in figure 20. This component is also embedded in isolation in order to minimize external heat transfer (not shown in figure).
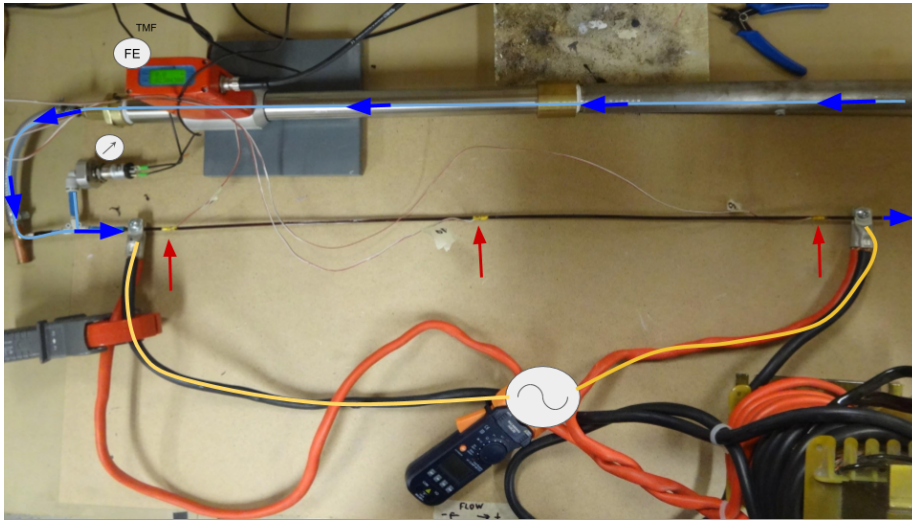
Figure 20: The setup used for the 880mm hollow conductor.

9.3   4-turn Hollow Conductor

Single flow

The setup used for the 4-turn single flow hollow conductor is similar to figure 20 apart from the conductor being wound around the bobbin as shown in figure 9. As the experiments are made the component is closed with a lid as shown in figure 21

Parallel flow

For the parallel flow, the ends of the bobbin are sealed and one side is pressurized thus generating the desired flow through each of the eight channels shown in figure 10. The setup is shown in figure 21. In this setup some flow was needed from the pressurized and out through the ends of the conductors (as illustrated in the right part of figure 21) to prevent overheating of these sections.
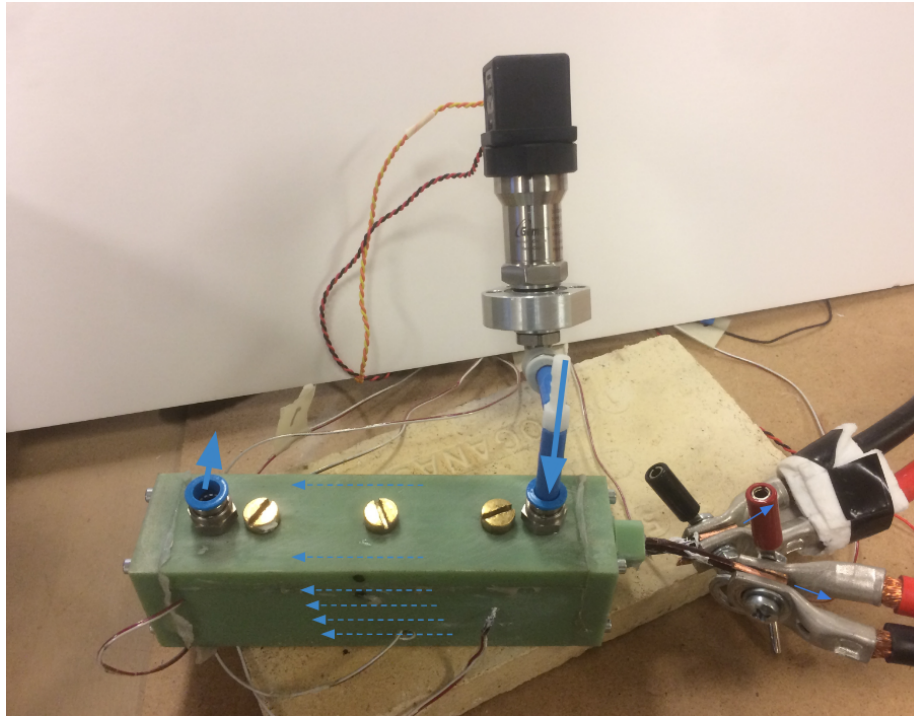
Figure 21: The setup used for the 4-turn parallel flow, note the flow through the connecting terminals on the right.

9.4   Equipment used

Flow meter

In order to accurately measure the required pump power for a given flow a flow meter is installed upstream of the pressure transducer. The output of the flow meter is 4-20mA which means that a shunt resistor must be used to generate a voltage which is in turn fed to the data logger. The flow meter outputs the volume flow in the unit m^3/h_n where the n stands for normal. This means that the volume shown is in a normal atmosphere of 1.01325 bar and 273K. Any calculations must therefore first convert this reading to the actual pressure and temperature.

Figure 22: The VPF R200.M100.D1 flow meter, image taken from [8]

Pressure transducer

The gems 3500 series is a pressure transducer for pressures in the range of 0-16 bar absolute pressure giving a proportional voltage output between 0-10 volts, see figure 23. The pressure transducer is mounted just upstream of the inlet to the conductor. The pressure read will therefore be equal to the pressure drop for the entire component.

Figure 23: The gems 3500 series pressure transducer used, image taken from [6]

J-type Thermocouple

In order to accurately measure the temperature of the components at its full range j-type thermocouples are used. The benefit of using these are their simplicity and wide temperature range. The agilent datalogger allows the user to connect the thermocouple directly and presents the temperature directly in degrees Celcius. In total 5 thermocouples are used at various locations of the components.

AC current meter

In order to accurately set and measure the heat load an AC clamp meter is used with its output voltage signal fed to the datalogger. The clamp meter can be seen in the lower left corner of figure 20.

Transformers

Two transformers are used in series to generate the required AC losses in the components, see figure 24. The transformers are set up to create a very low voltage with a high current with a variable transformer allowing the heat load to be set to any value within the transformers current limit.

Figure 24: The transformers used to generate the required heat loads.

Agilent Datalogger

Figure 25: The Agilent datalogger used, image taken from [7]

The Agilent Datalogger is used to conveniently collect all the measurements into a single .csv file. The datalogger is capable of scanning up to 250 channels per second depending on the connecting board used. Using the logger in conjuction with the BenchLink interface allows for live overview of the results as shown in figure 26.
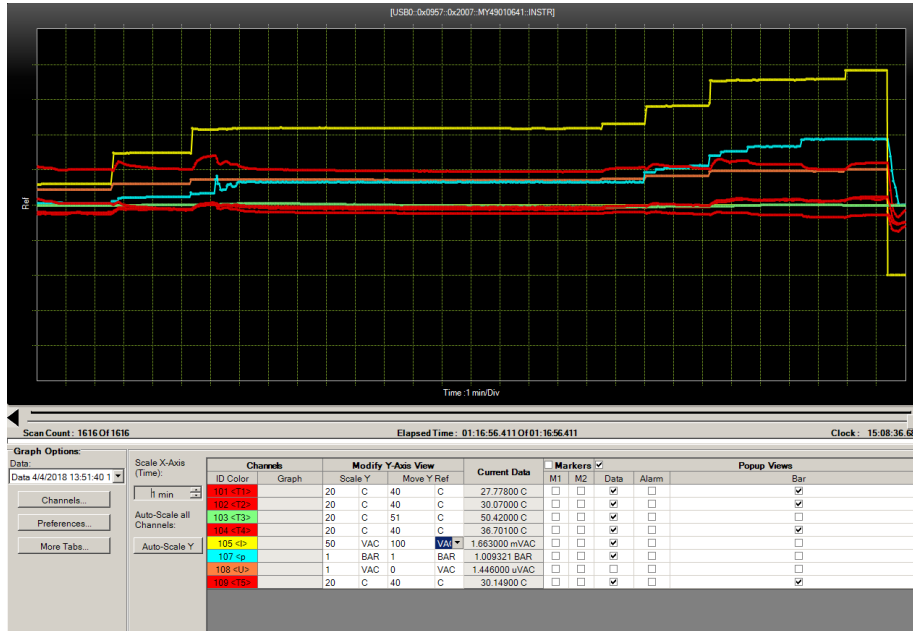
Figure 26: The BenchLink interface used together with the datalogger

9.5 Measurement errors

Apart from the worst-case scenario of the flow meter the measurement errors are considered within acceptable range.

	Best Case	Worst Case
Data logger DC voltage		< 0.1 mV
Data logger AC voltage		~ 1 mV
J-Type Thermocouple		$\pm 2.2°$ C
Pressure Transducer		± 40 mBar
Flow Meter	$\pm 1 m^3/h_n$	$\pm 10 m^3/h_n$

Table 1: Measument errors of the equipment used

9.6 Data Collection

With the data logger connected to all of the equipment each of the aforementioned component are subjected to varying heat loads and inlet pressures. During the experiments care is taken not to overheat the copper or any other heat sensitive equipment. The 200mm copper tube and the 4-turn parallel flow are both thermally limited to 100°C by the materials used in the setup (the thermal insulation of the 200mm tube and the silicon used in sealing the bobbin of the 4-turn component). Due to the long time constants of the bobbin experiments on the 4-turn component are carried out in sequences of constant temperature to shorten experiment times.

9.7 Inductance measurement

In order to verify that the losses generated are purely resistive measurements will be made on a set of components using an LCR meter to assess the inductance and resistance.

Component	Description
4tc	4-turn tightly wound, as shown in figure 9
5tc	As above but with one extra turn.
5to	As the 5tc but loosely wound with a 5mm air gap between each turn.
6x6	A 6x6mm test length of hollow conductor wound one turn.

Table 2: Components used in LCR measurements.

10 Results

This section is divided into 7 subsections. The first two subsections present the results for each of the components examined together to facilitate comparison of the different methods used and components studied. The last five subsections contains interesting results related to the method used. All of the results are discussed in section 11. More detailed versions of the figures presented in the first two sections can be found in appendix A.

10.1 Summary of results

The following figures presents the results for each component. Each figure presents the results for a given component from each of the three methods next to each other where the first column presents the data obtained from experiments, the second column shows calculated results using the mathematical model and the third column shows results from the FE simulations. The top row of each figure describes the maximum copper temperature for a given inlet pressure and current density and the second row describes the maximum copper temperature for a given heat load and pump power.

200mm copper tube
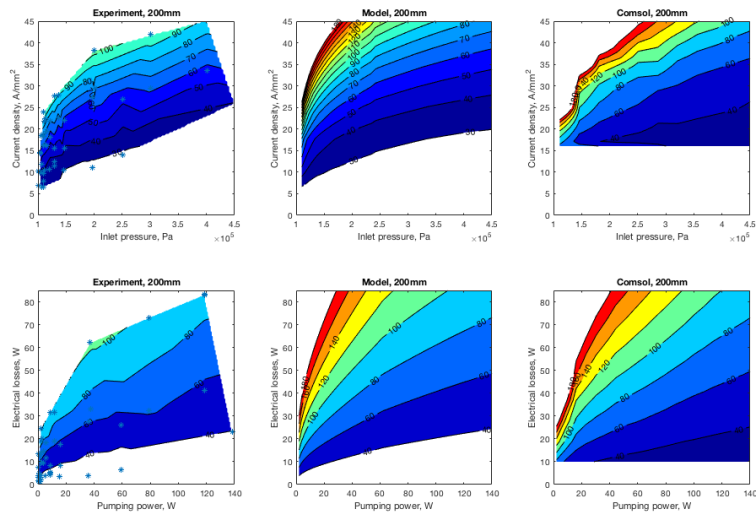
Figure 27: Comparison of results, 200mm copper tube

The experiments made were limited to a maximum temperature of 100°C which means that the full potential of this conductor was not examined completely. The experimental results does however agree reasonably well with the mathematical model, showing that current densities well above 30A/mm² are possible at relatively low inlet pressures. The finite element results in the third column are somewhat irregular which is discussed further in the following section.

880mm hollow winding
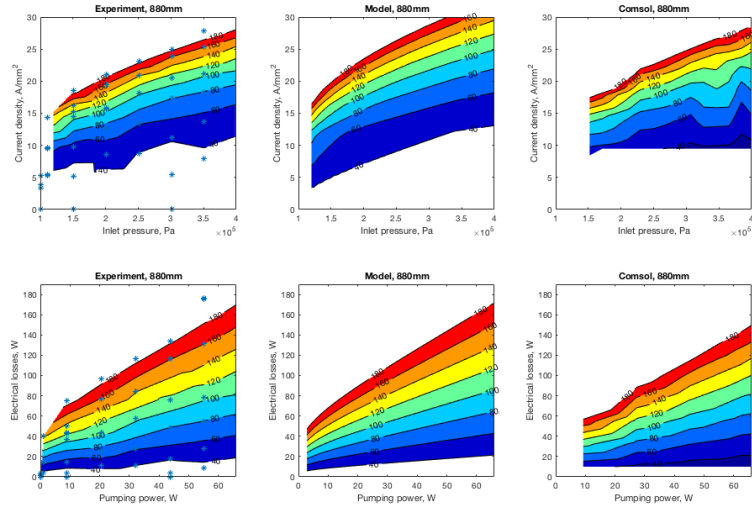
Figure 28: Comparison of results, 880mm hollow winding

As expected, the 880mm hollow winding does not perform as well as the shorter copper tube for a given inlet pressure. This is mainly due to two reasons, firstly the longer pipe length means higher friction thus reducing the flow velocity for a given inlet pressure and secondly the temperature of the cooling fluid increases as it absorbs heat along the windings length. As the temperature of the fluid increases the heat flux from the copper to the fluid decreases meaning less cooling of the copper. During the experiments made, the maximum current density of this component was never able to exceed $30A/mm^2$. It should however be noted that because of the reduced volume flow, the theoretical pumping power is also lower compared to the shorter copper tube.

1250mm 4-turn single flow
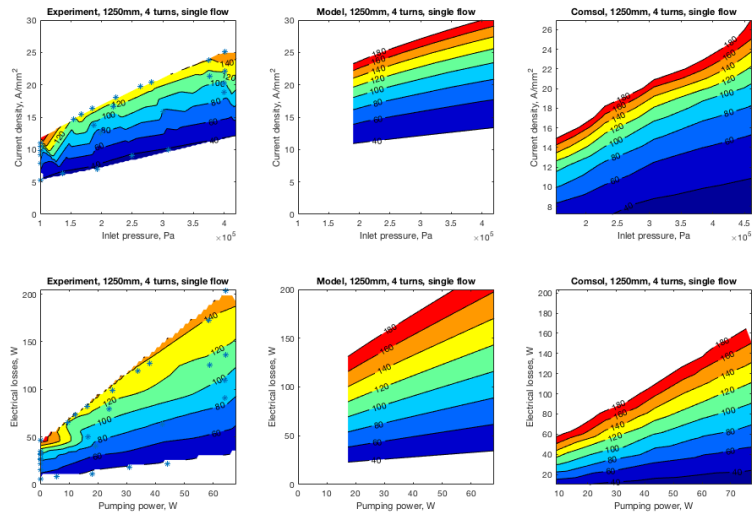
Figure 29: Comparison of results, 1250mm 4-turn hollow winding, single flow

The 4-turn single flow winding shows similar characteristics to the 880mm winding. Although this component features a longer channel for the fluid to pass through, the external heat transfer is improved due to the thermal contact to the inside its bobbin, see figure 9.

1250mm hollow conductor 4 turns parallel flow

The parallel flow component was only examined through experiments and therefore only two figures are presented.
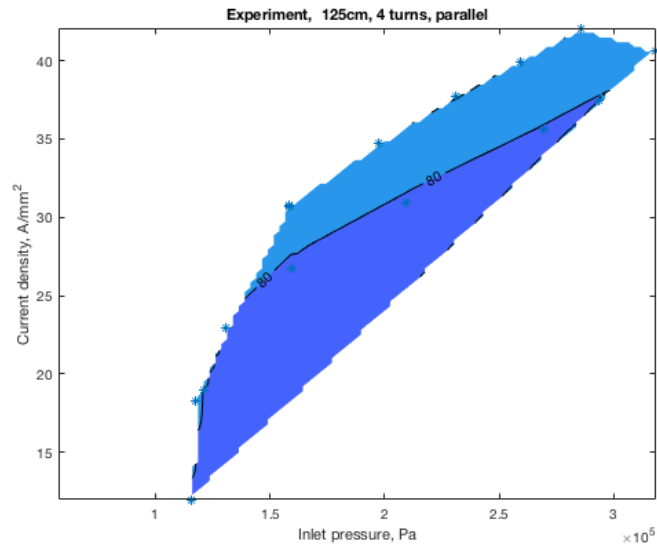
Figure 30: Experiment results showing current density versus inlet pressure
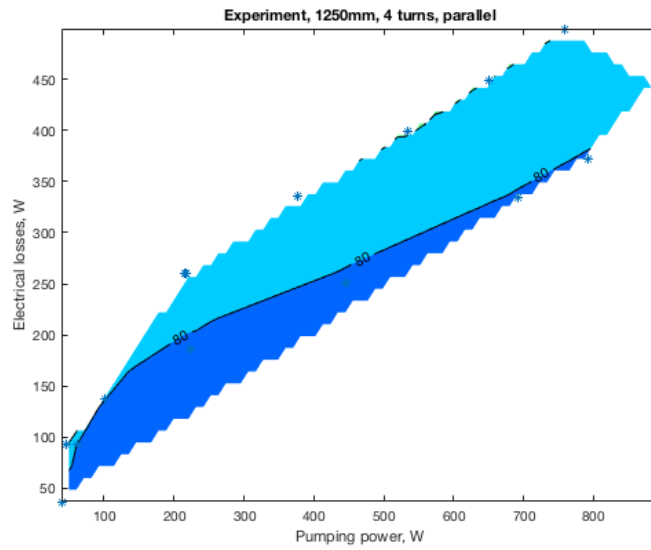
Figure 31: Experiment results showing heat load versus pump power

This component shows similar characteristics to the short pipe section and in figure 71 we see current densities well above $30A/mm^2$ at relatively low pressures. Due to the sealant used in the setup shown in figure 29, the experiments were limited to $100°C$. The results does show nonetheless a significant increase in maximum current densities at the inlet pressures used. Because this compo-

nents consists of 8 parallel channels, the theoretical required pumping power is increased by a factor 8 compared to the short pipe section for the same pressures. This can be seen in figure 72 where theoretical pumping powers up to 800W are used.

10.2   Comparison of results

In order to facilitate comparison between the different components the following two figures compares the experimental results of each of the four components next to each other.
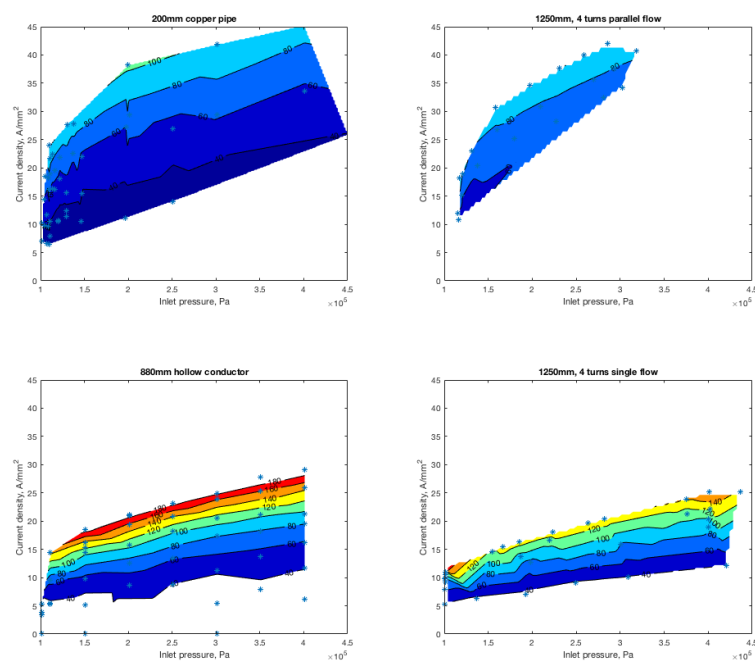
Figure 32: Comparison of the four components on same axis scales, current density versus inlet pressure.
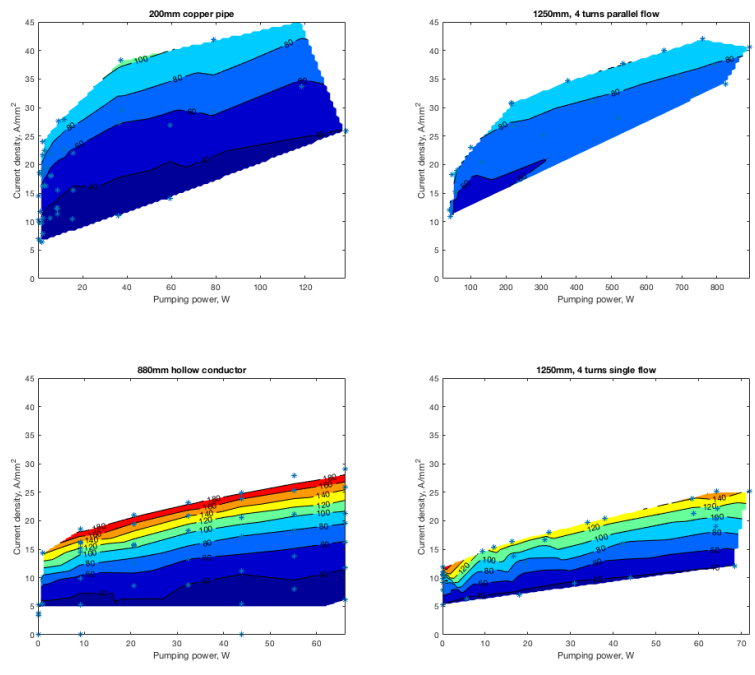
Figure 33: Comparison of the four components, current density versus pump power.

As the parallel flow component consists of 8 short channels the following figure shows the experimental results from the 200mm copper pipe and the 1250mm parallel flow component where the pump power of the latter has been divided by the number of channels.
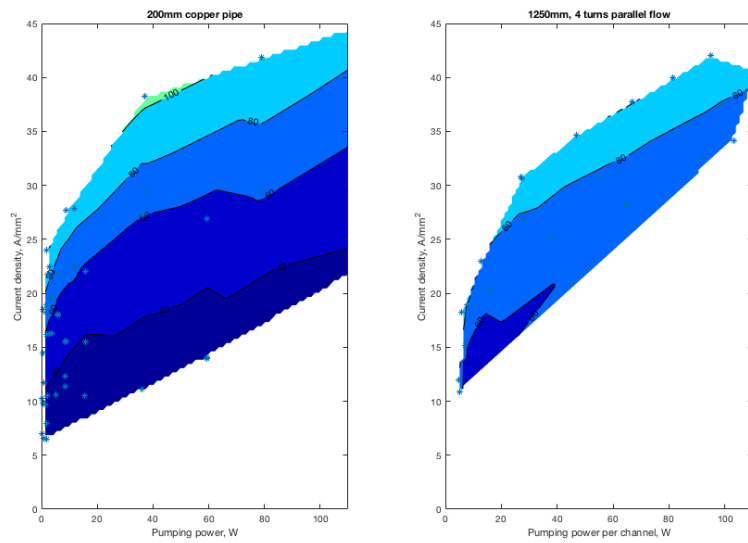
Figure 34: Comparison of the 200mm copper tube and 4-turn parallel flow, current density versus pumping power per channel.

Single or parallel flow

In order to enable a more accurate comparison between the 4-turn single flow and parallel flow component the experimental results from each are presented next to each other in figure 35 using the same axis limits.
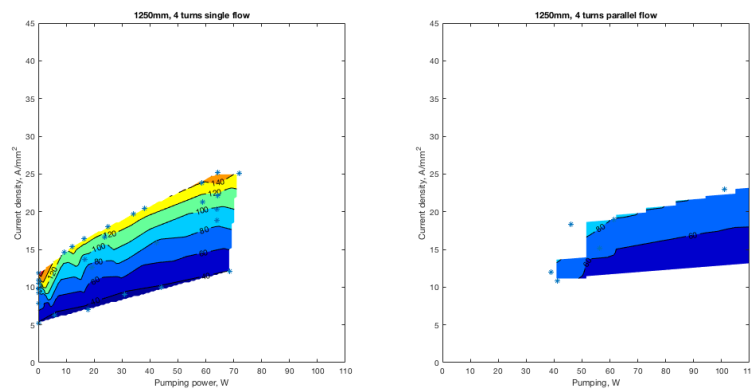
Figure 35: Comparison of 4-turn single and parallel flow using same axis limits, current density versus pump power

41
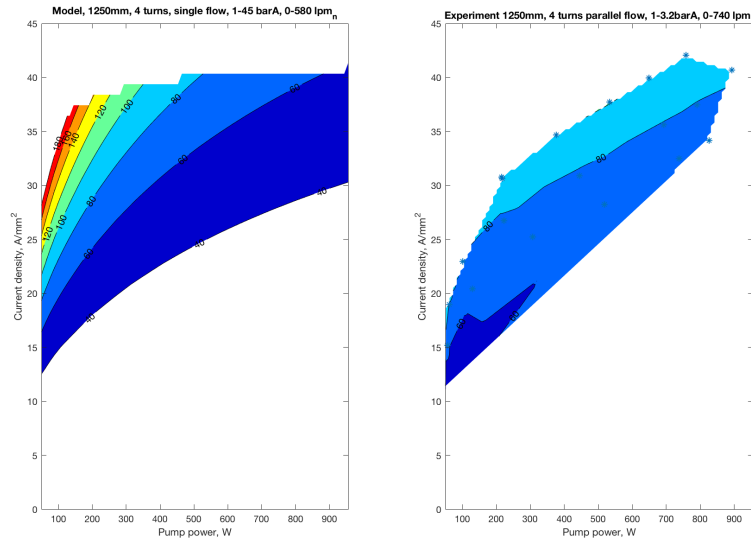
Figure 36: Comparison of 4-turn single flow model versus 4-turn parallel flow experiment, current versus pump power.

To further compare the 4-turn single flow with its parallel flow counterpart the mathematical model is used to examine the single flow component in the same regions as the parallel flow component. Although the cooling performance of the two components appear similar given similar inlet pressures, in order to achieve similar pumping powers in the single flow system very high pressures up to 45 bar must be used, as shown in figure 36.

10.3   FE Analysis

PFM

The pipe flow module was only successful in producing results for oil as cooling fluid and an example of results using this module are shown in figure 37. In order to enable more experiments no further efforts were made using this module.
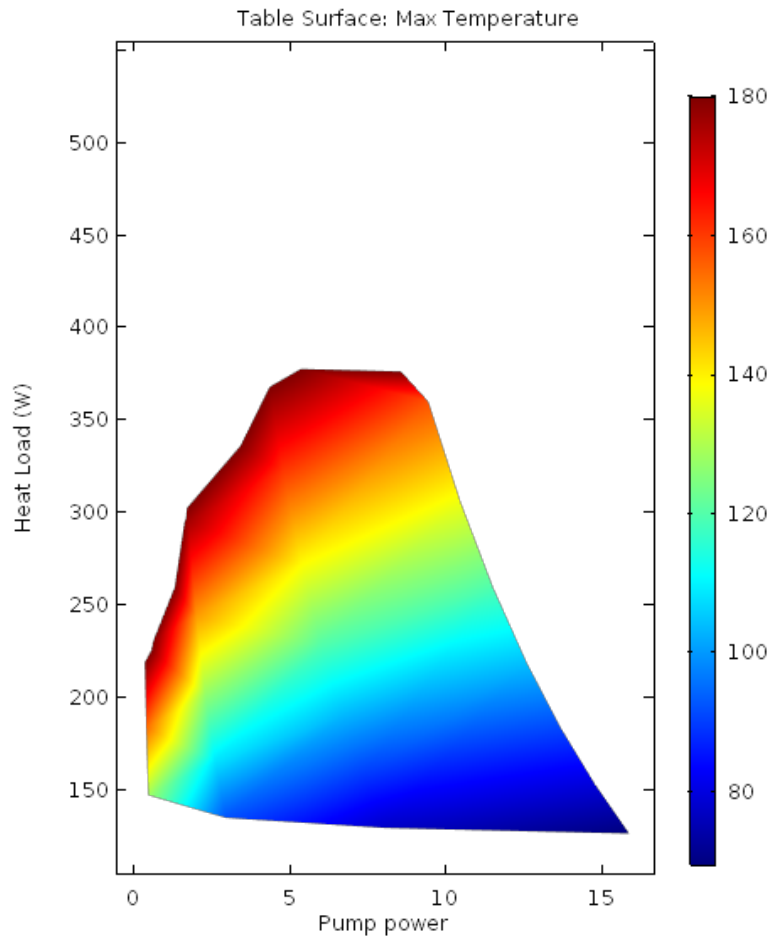
Figure 37: Comsol results using pipe flow module with oil as cooling fluid.

Flow velocities

In order to determine the accuracy of the used turbulence model the flow velocities for the 1250mm hollow conductor are presented in figure 38. This figure shows the fluid velocity at the pipe center along the pipe length.
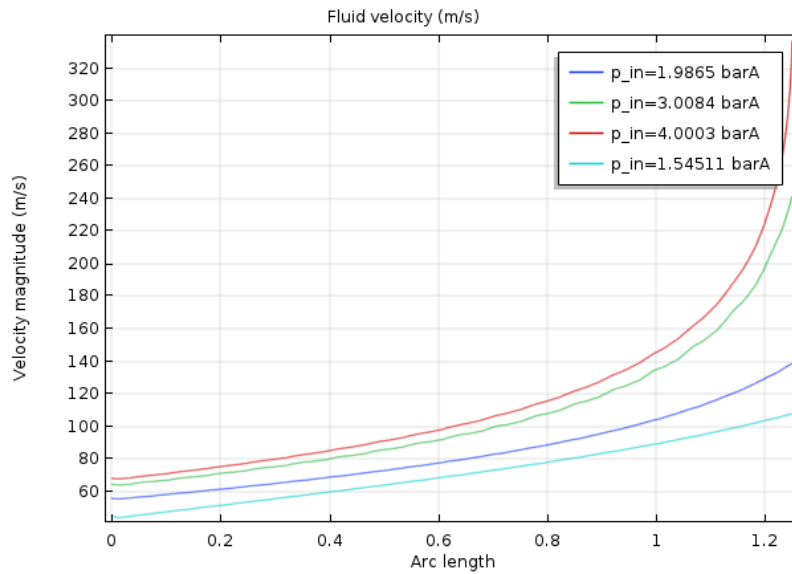
Figure 38: Comsol results showing typical flow velocities for simulations made on 1250mm component.

The model is not intended for velocities greater than Mach 0.3 which many of the simulated cases are well above as shown in figure 38, this is discussed further in section 11.2.

Heat load vs pump power

To compare the pump power calculated by the mathematical model to the pump power calculated by comsol figure 39 shows the maximum temperature of the copper at a given pump power as calculated by comsol at a given heat load.
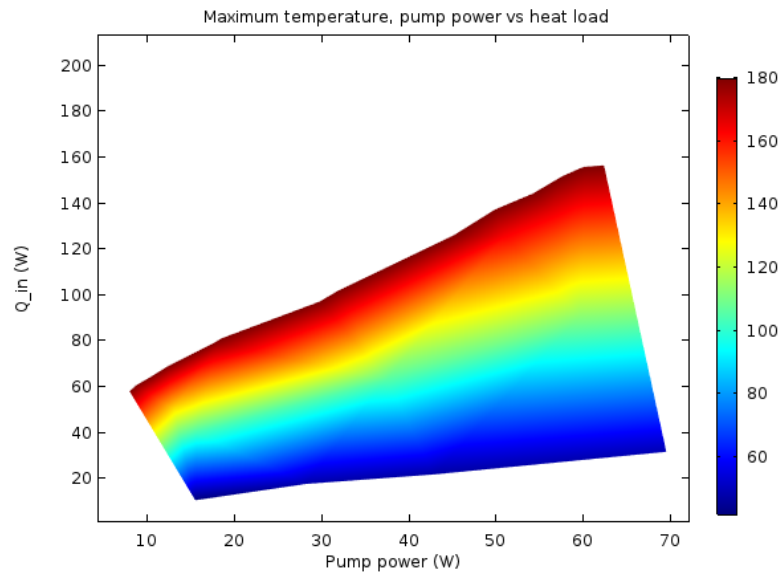
Figure 39: Comsol results showing heat load versus pump power calculated by comsol

10.4 Flow measurements

Some interesting results from the flow meter used are presented in this section.

Leakage

The flow meter proved useful in evaluating the effectiveness of attempts made to seal leakages in the system, as presented in figure 40.
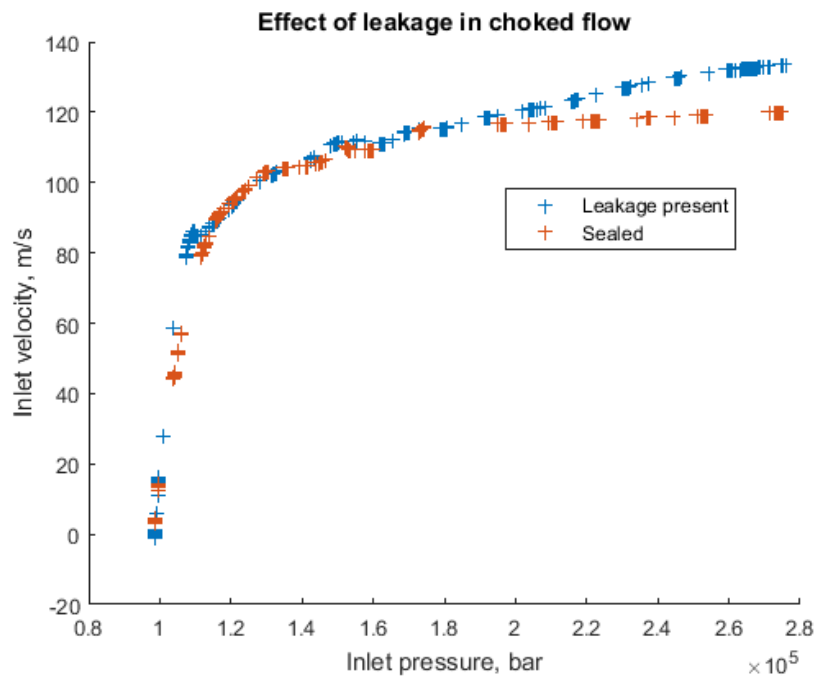
Figure 40: Effect of leakage on measurement.

As shown in the figure, the measured inlet velocity decreases after the leak has been sealed.

Flow meter evaluation

Figure 41 and 42 shows the difference between the measured flow values and the calculated flow values. Figure 42 also presents the error bars for the best- and worst case measurement errors in inlet velocity measurements.
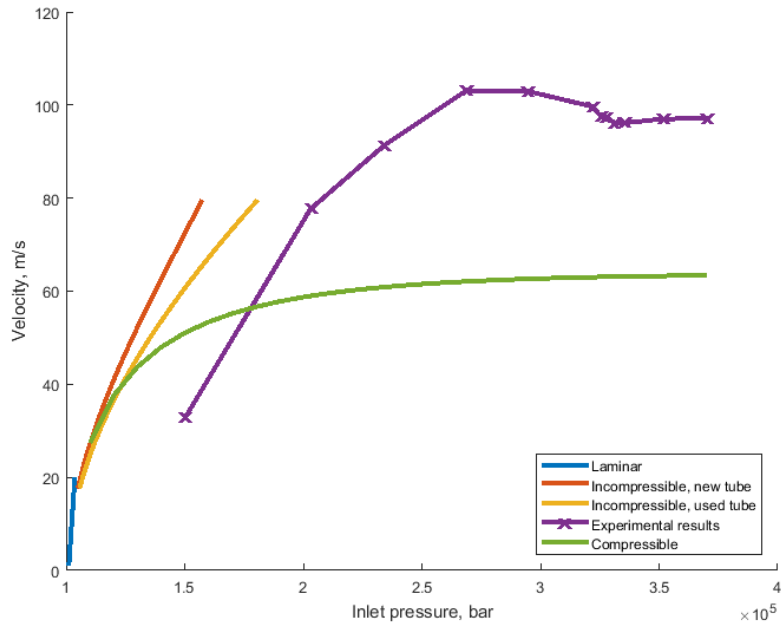
Figure 41: Flow measurements compared to model results.
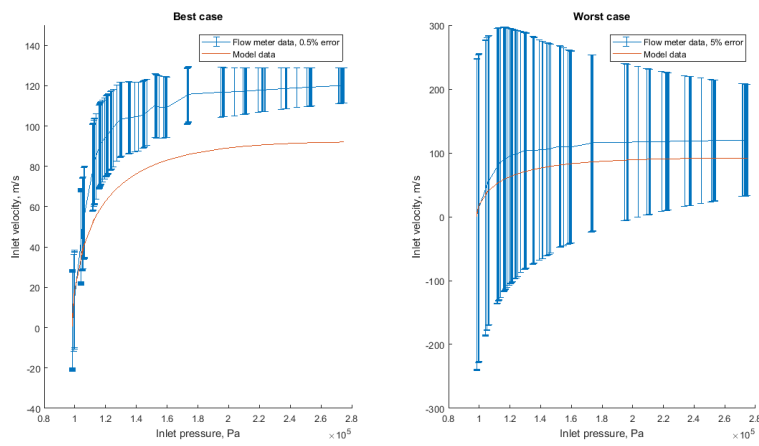
Figure 42: Flow measurements with error bars compared to model results.

The error ranges of the flow meter indicate that the measurements are most likely not useful in this application as the volume flows are too small. This is discussed further in section 11.1.

10.5 Overheated conductor

During the experiment phase of the project a hollow conductor was exposed to temperatures well above the limits of the insulating material with the results shown in figure 43.

Figure 43: Copper insulation subjected to ∼250°C next to unused conductor.

10.6 Thermal imaging

A thermal camera was used during the experiments to visualize the heating and cooling of the components. Two images are included showing the thermal distribution of the 4-turn single flow.
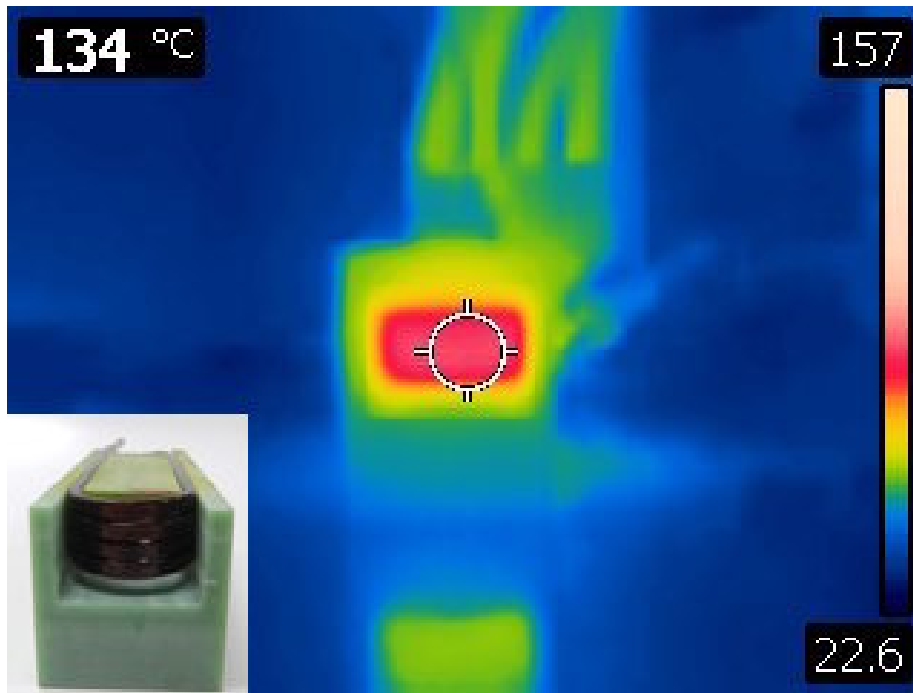
Figure 44: Thermal image of end windings without cooling, 4 turn serial flow

As can be seen, the winding is heated uniformly to a temperature of roughly 134°C with the surrounding bobbin absorbing some of the heat load.
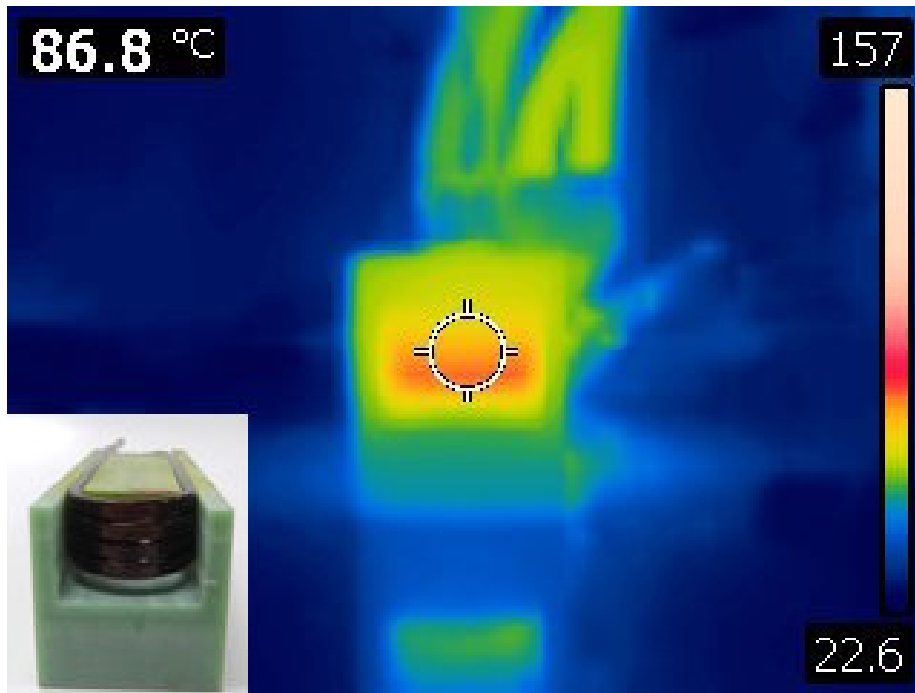
Figure 45: Thermal image of end windings with cooling, 4 turn serial flow

Once the cooling is applied, the temperature distribution shifts and the top windings where the air enters are now cooler than the bottom.
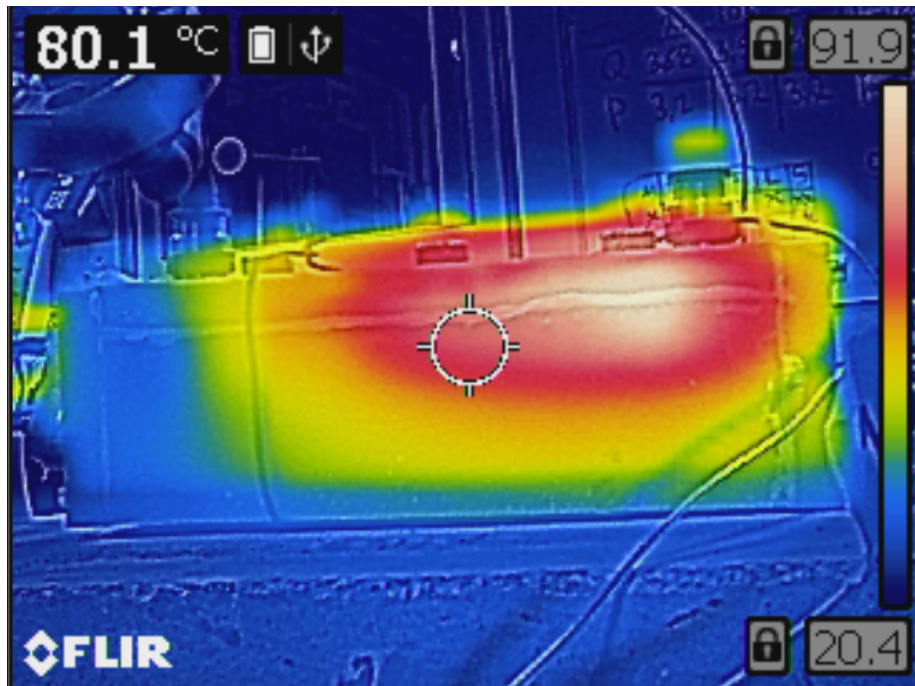
Figure 46: Thermal image of bobbin with cooling, 4 turn parallel flow

Figure 46 shows the temperature distribution of the outer casing of the 4-turn parallel flow where the cooling fluid enters through the left port and exits from the right port on top of the component.

10.7 LCR measurements

To assess the inductance of the components the measurements form the LCR machine is presented below showing the inductance in the region 2Hz-200'000Hz.
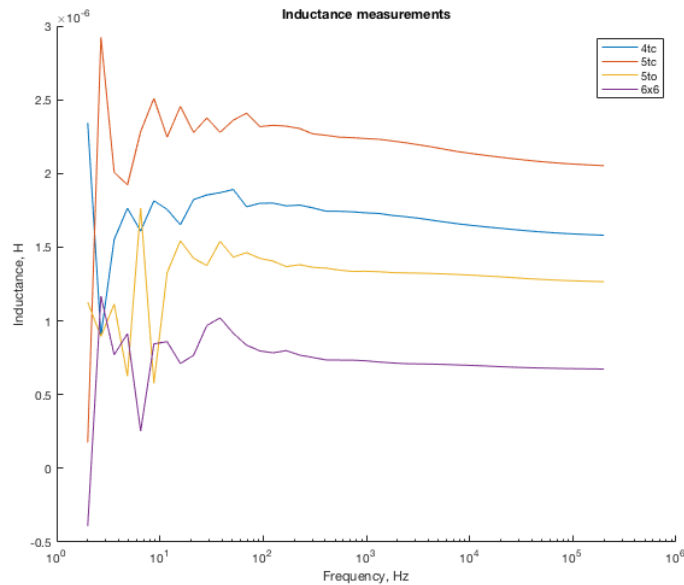
Figure 47: Inductance measurements of four different components.

As predicted, the inductance of the components used are small in relation to the resistive losses of the copper conductors. At 50 Hz the measured inductance of the 4-turn component was about $1.7*10^-6$H which can be regarded as negligible in relation to the resistance.

11 Discussion

11.1 Flow Measurement

Leakage

Whenever dealing with pressurized flow any leakage possibilities must be addressed. When measuring the inlet velocity of a component some results were found to be unreasonable. Figure 40 shows the inlet velocity gradually increasing although the flow is clearly choked. After a close examination of the component a small leakage was found at the intersection between the hollow conductor and the pneumatic piping. Once the leak was sealed new measurements were made with more reasonable results.

Accuracy

The datasheet of the flow meter dictates a worst case accuracy of $\pm 5\%$ of full scale. Figure 42 shows the inlet velocity difference between the measured values from the flow meter and the calculated values. The manufacturer states that the best case accuracy is obtained through annual ISO calibration and through the use of a special tubing kit. Although the tubing kit is used the instrument has

not been calibrated according to schedule, meaning that the measured values are of little use when measuring in such low regions of the instruments full scale.

11.2   FE Analysis

The results from Comsol multiphysics agree reasonably well with the results for the 200mm component but as the length of the flow increases the results are no longer as accurate. A probable cause for the discrepancy lies in the turbulence model used. The model is not intended for velocities greater than Mach 0.3 which many of the simulated cases are well above as shown in figure 38. Another contributing factor to the discrepancy of the 1250mm singel flow results is the geometrical difference between the experimental setup and the simulated. Because a 2-dimensional axisymmetric model is used the component is simulated as a straight pipe.

11.3   PFM

The pipe flow module failed to generate reasonable data using air as fluid, this is probably due to the general difficulties involved with simulating compressible flow at high velocities. This module does however seem very useful for analyzing cooling performance of an oil- or watercooled system.

11.4   Mathematical model

Once the model is updated with measured external heat transfer coefficients the results are within reasonable limits compared to the experimental data. Due to the more complex geometry of the 1250mm 4-turn component the external heat transfer coefficient is difficult to estimate which is a probable cause to the slight discrepancy between the model and experiment results. Due to lack of time no mathematical model has been made for the 4-turn parallel flow.

Accuracy

Expected accuracy of the empirical models used when calculating the heat transfer coefficient varies greatly and literature describe the models as "reasonably accurate" [2]. The model used is a result of several attempts to create an accurate model solving both the fluid mechanics and the heat transfer of the system simultaneously. This is difficult as almost all of the fluid properties are temperature dependent and all of the heat transfer properties are flow dependent. The present model uses some iteration to address this but the flow chart described in figure 17 is an accurate representation of the algorithm used. The result of not evaluating the fluid mechanics with updated fluid temperatures is difficult to estimate but figure 58 and 39 shows little difference between the calculation of pump power by mathematical model or comsol.

11.5   Experimental data

Estimating pump power

Due to the flow measurement inaccuracies described in section 11.1 the measurements from the flow meter are discarded. Instead the mathematical model

is used to derive pumping power from the measured inlet pressures. Because of this all pumping powers shown in the results are derived from the mathematical model and thus hard to validate apart from the comparison made with figure 70 and 39.

Cooling similarities

As expected the 200mm copper pipe and the 4-turn parallel flow components shows similar cooling characteristics in relation to inlet pressures, see figure 32. Although the channels are shorter in the parallel flow setup (125mm each) the maximum temperature is still higher than the corresponding temperatures of the 200mm component. A probable reason for this is the lack of cooling flow through the conductor portion between the exit holes, see figure 10.

The 880mm and 1250mm single flow components also show similar characteristics with higher temperatures in the longer component.

11.6   Single vs Parallel flow

Judging by figure 33 the parallel flow seems to allow for the highest current densities while still keeping the maximum temperature below 100°C. Looking at the pump power in this figure it is difficult to draw any conclusions as the single flow experiments were only made up to roughly 70W of pump power while the parallel flow experiments were made up to over 800W. Figure 35 compares these two components with similar axes and from this perspective the difference is no longer as apparent. Using the mathematical model of the serial flow, predictions can be made on the performance at higher pump powers which is shown in figure 36. In this figure the cooling performance of the single flow seems to outperform the parallel flow for a given pump power. However, in order to reach such pump powers an inlet pressure of 45 bar is needed which is well above the capabilities of any compressor found in the hardware stores and is therefore not considered practical. The parallel flow on the other hand requires a relatively low pressure of 3.2 bar and a flow of 740 lpm_n which is within the operating range of a standard compressor.

11.7   Compressor

It is worth mentioning that the compressed air used in this work has a constant temperature of around 20°C. In a hypothetical system with a compressor connected directly to an electrical machine the temperature of the compressed air would not be constant and likely much higher due to the heating of the air as it is compressed.

12   Summary

The results of the four analyzed setups indicate that current densities above 45 A/mm^2 are possible using a hollow conductor with parallel flow from one end of the winding to the other with flow characteristics within reachable levels. It is also concluded that simple models and components can be used to initially predict the cooling capabilities of more complex systems.

13 Further studies

The work done during this master thesis project is only a scratch on the surface of the directly cooled winding possibilities. Figure 48 shows two different future paths where one is the advancement to a system scale of the current studies and the other is a study of alternative cooling fluids such as water or oil.
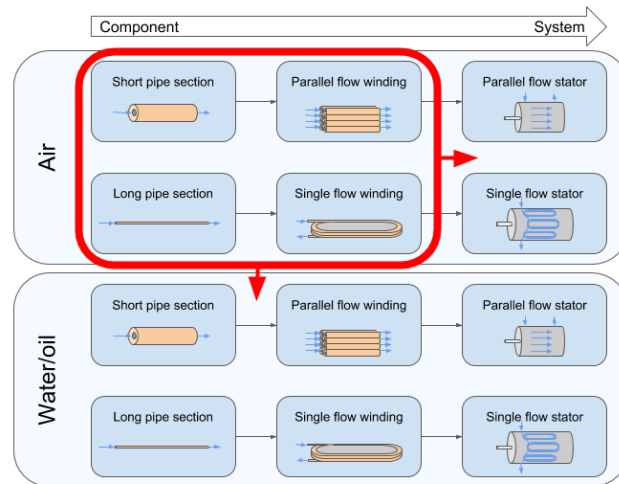

Figure 48: Overview of the area of this work and two interesting directions for further studies.

13.1 Prediction of oil cooled windings

Through slight alterations to the mathematical model used in this work a coarse prediction of the cooling performance using oil as cooling fluid is made. The model is run on the different components of this work for comparison and the results shown below indicate some interesting performance, especially for the parallel flow scenario. Calculations have been made with up to 70 bar as maximum inlet pressure.
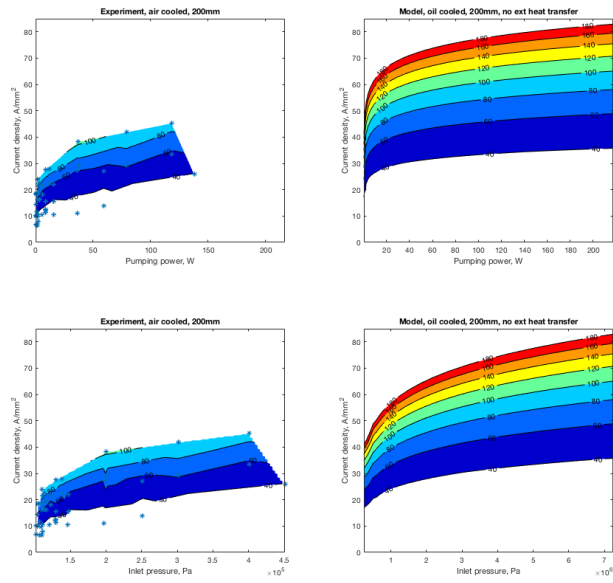
Figure 49: Estimation of oil as cooling fluid for 200mm pipe
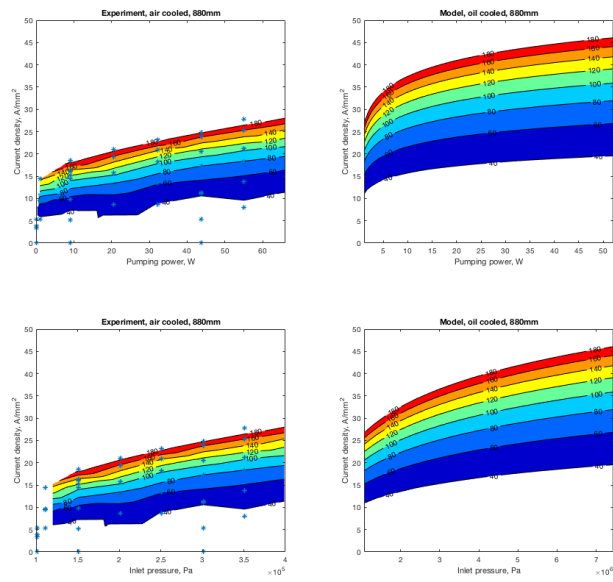
Figure 50: Estimation of oil as cooling fluid for 880mm conductor
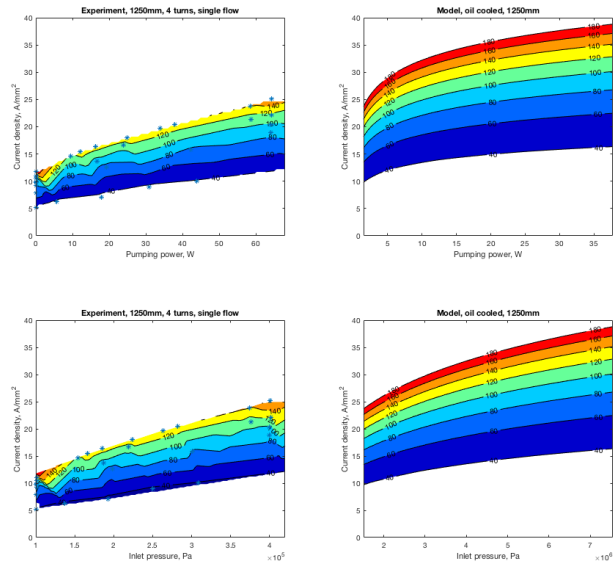
Figure 51: Estimation of oil as cooling fluid for 1250mm winding, single flow
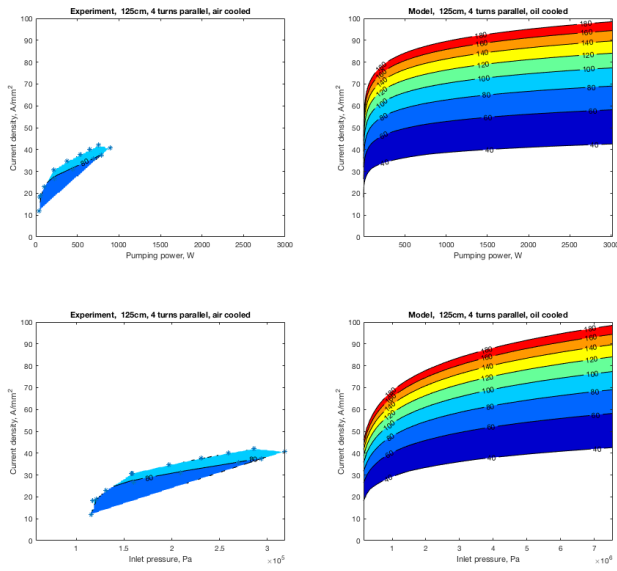
Figure 52: Estimation of oil as cooling fluid for 1250mm winding, parallel flow

14 Appendix A

14.1 Expanded Results

FE Analysis

The results from the comsol simulations are presented in this section with two figures for each component: the first figure for each component describes the maximum copper temperature for a given inlet pressure and current density and the second figure describes the maximum copper temperature for a given heat load and pump power.
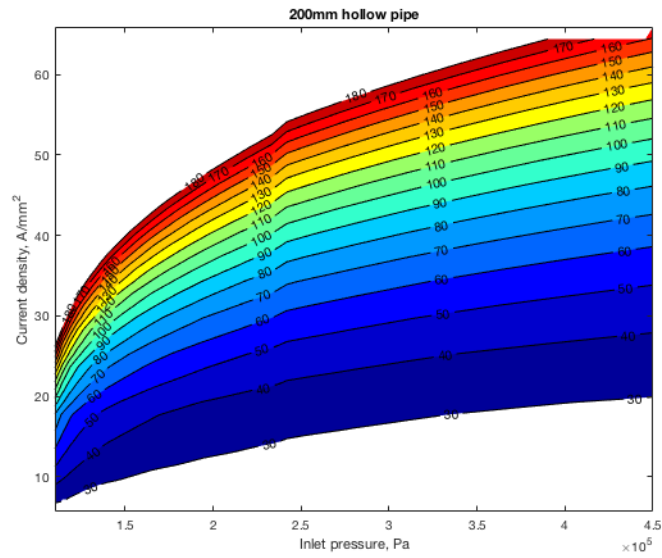
200mm copper pipe
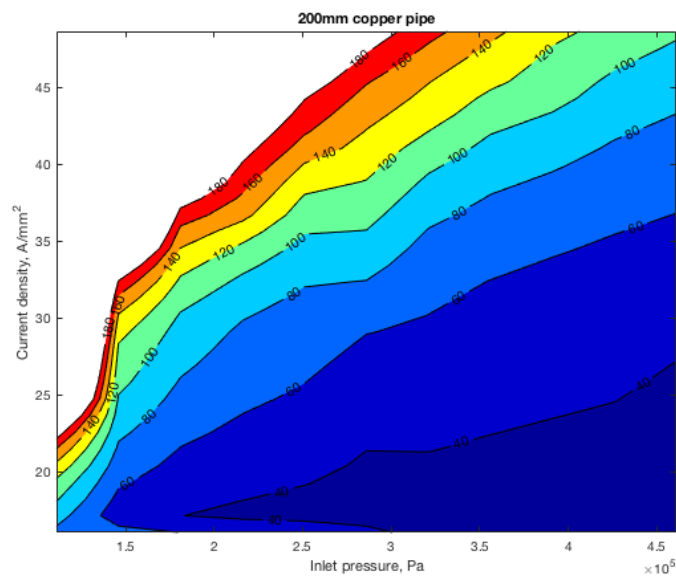
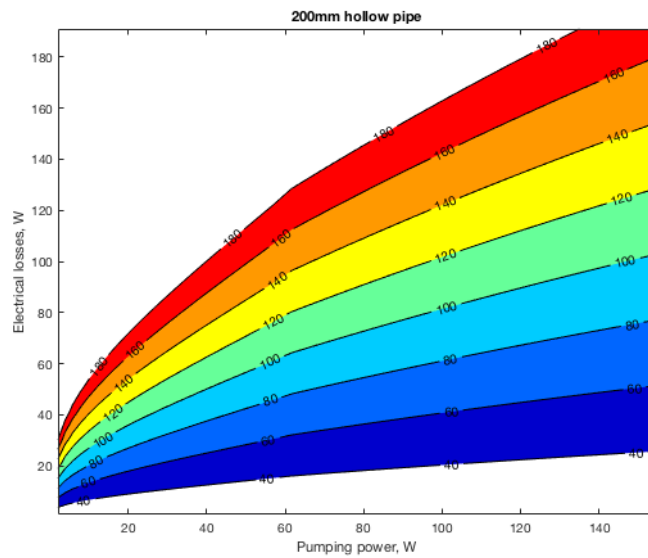Figure 53: Comsol results showing current density versus inlet pressure
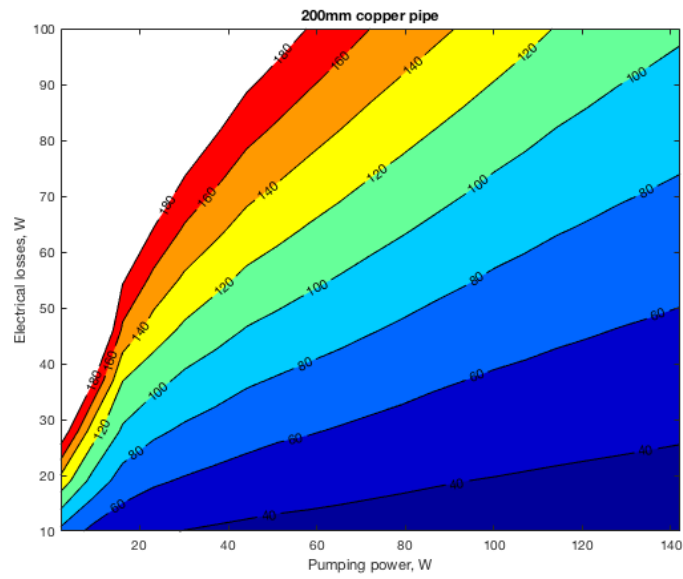
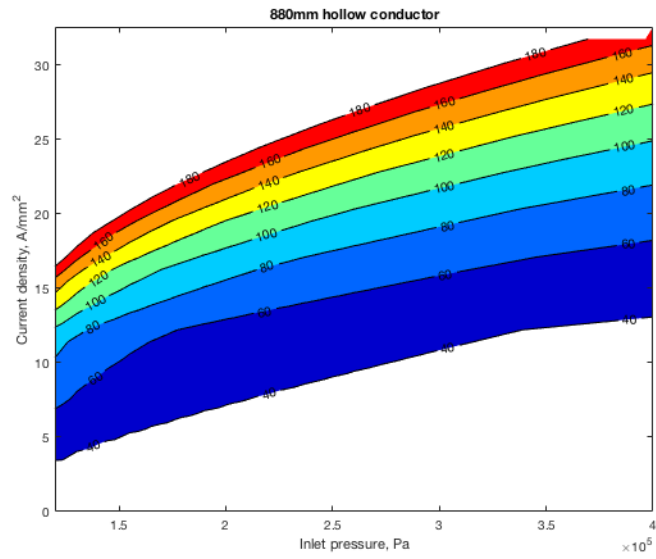Figure 54: Comsol results showing heat load versus pump power

880mm hollow conductor
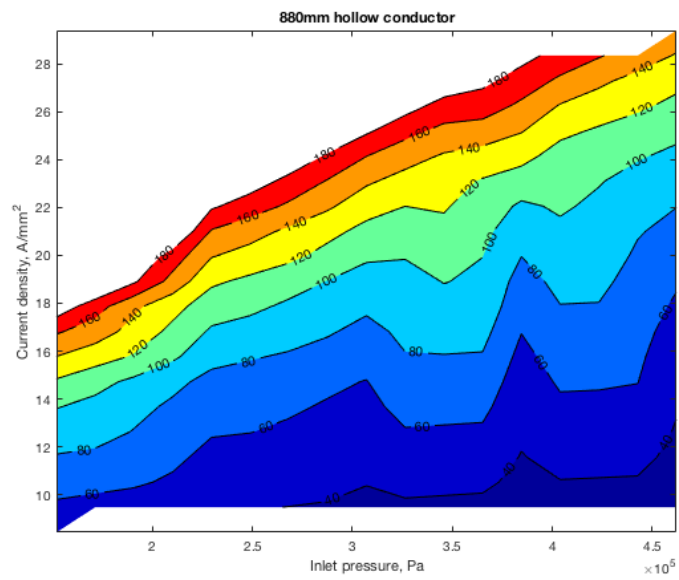
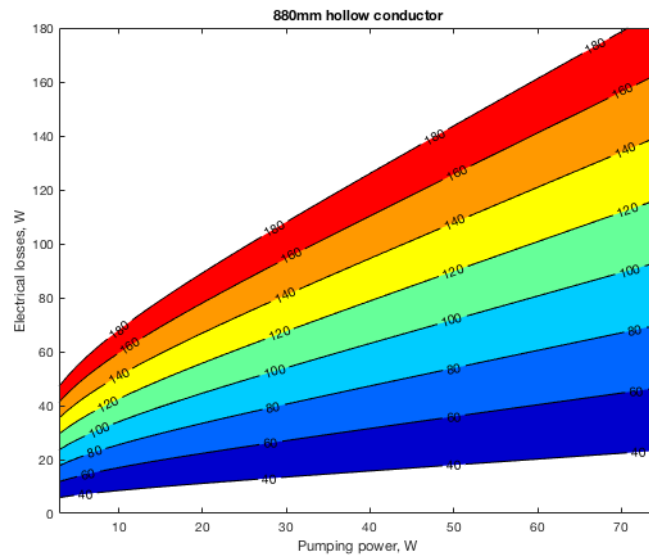Figure 55: Comsol results showing current density versus inlet pressure
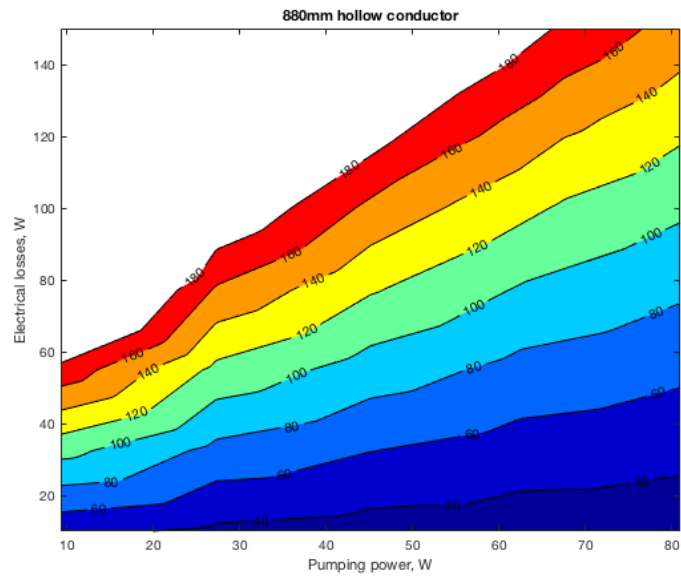
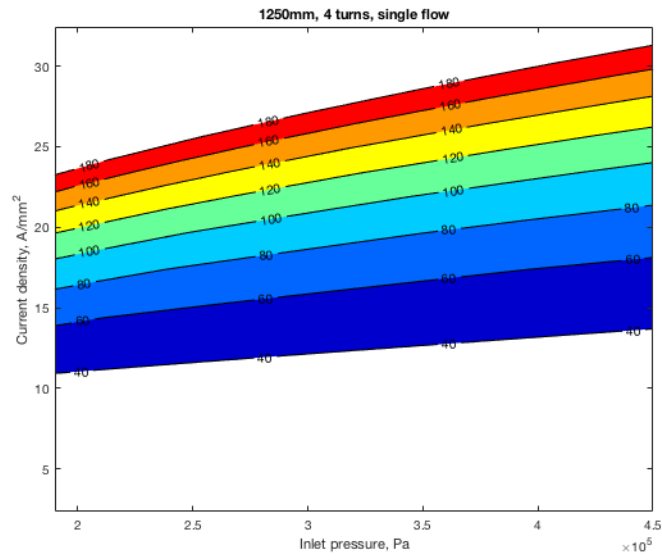Figure 56: Comsol results showing heat load versus pump power

1250mm hollow conductor
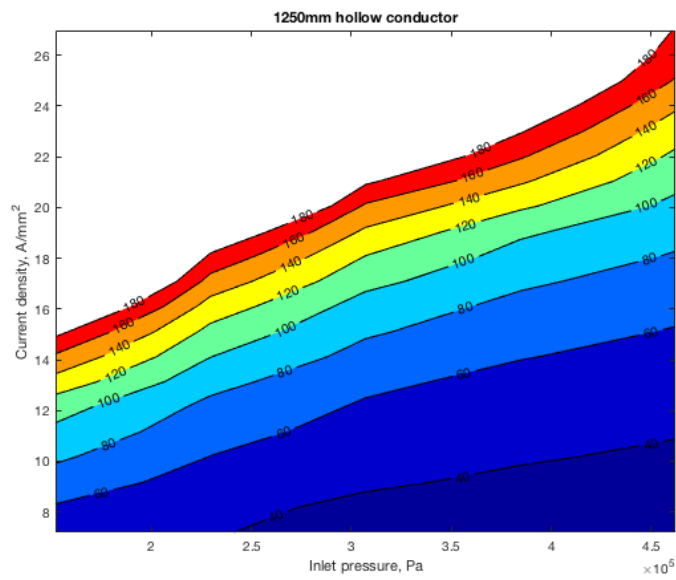
Figure 57: Comsol results showing current density versus inlet pressure

60
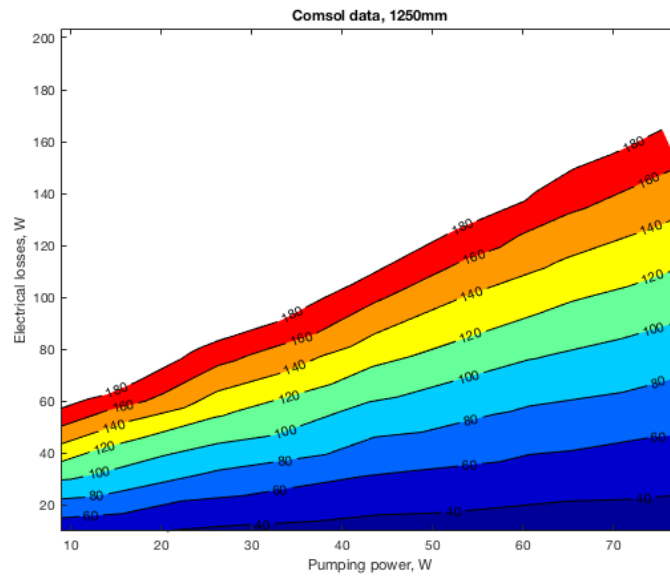
Figure 58: Comsol results showing heat load versus pump power calculated using mathematical model

Model Results

In order to allow for easy comparison, the results from the mathematical model are presented in the same way as the other two methods for each of the components. Each component is described using two figures where the first describes the maximum copper temperature for a given inlet pressure and current density and the second figure describes the maximum copper temperature for a given heat load and pump power.

200mm copper pipe

Figure 59: Model results showing current density versus inlet pressure

Figure 60: Model results showing heat load versus pump power

880mm hollow conductor

Figure 61: Model results showing current density versus inlet pressure

Figure 62: Model results showing heat load versus pump power

1250mm 4 turns single flow

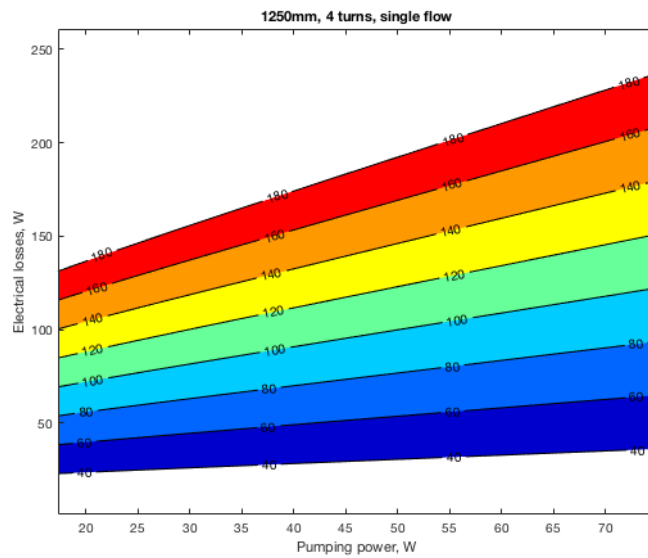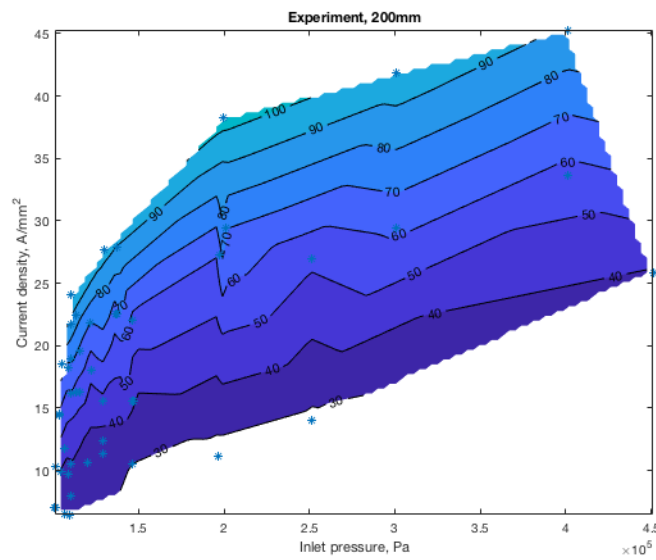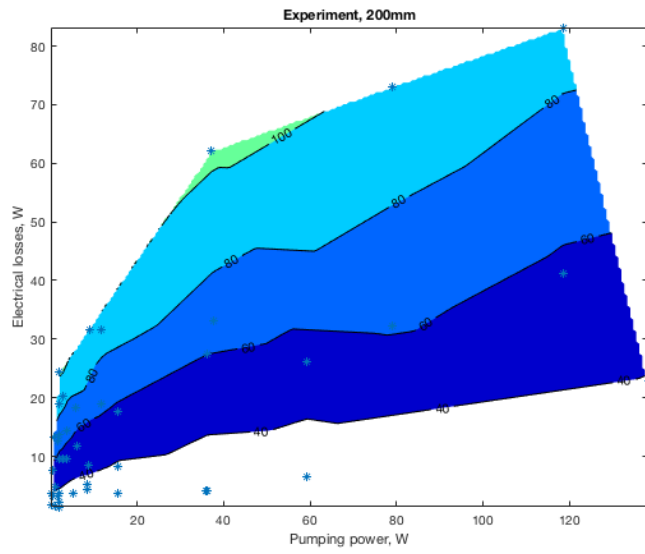Figure 63: Model results showing current density versus inlet pressure

Figure 64: Model results showing heat load versus pump power

Experiment Results

In order to allow for easy comparison, the results from the experiments are presented in the same way as the other two methods for each of the components. Each component is described using two figures where the first describes the maximum copper temperature for a given inlet pressure and current density and the second figure describes the maximum copper temperature for a given heat load and pump power.

200mm copper pipe

Figure 65: Experiment results showing current density versus inlet pressure

Figure 66: Experiment results showing heat load versus pump power
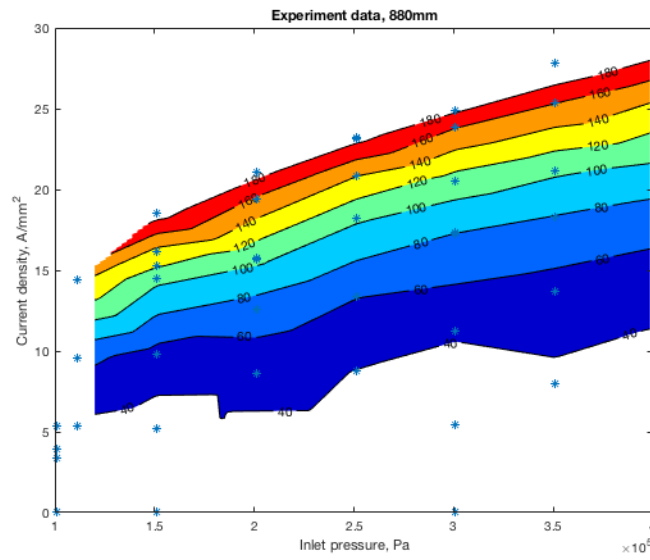
880mm hollow conductor

Figure 67: Experiment results showing current density versus inlet pressure
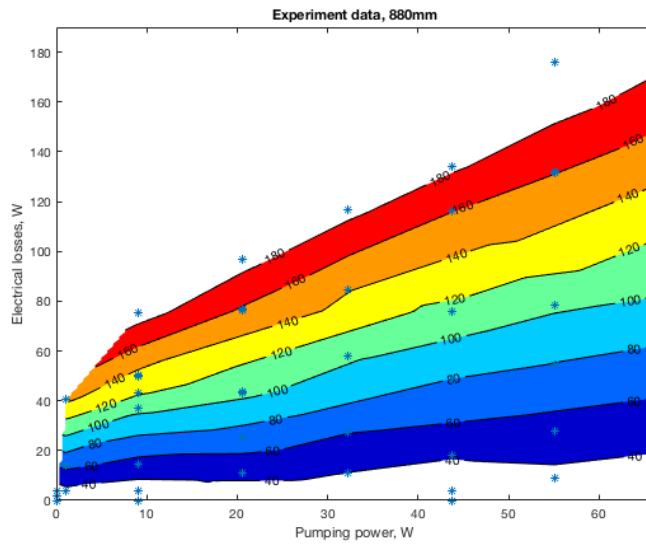
Figure 68: Experiment results showing heat load versus pump power

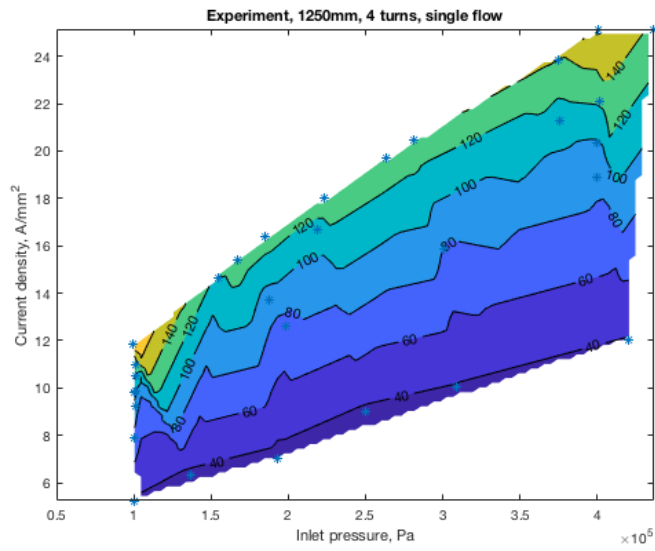**1250mm hollow conductor 4 turns single flow**

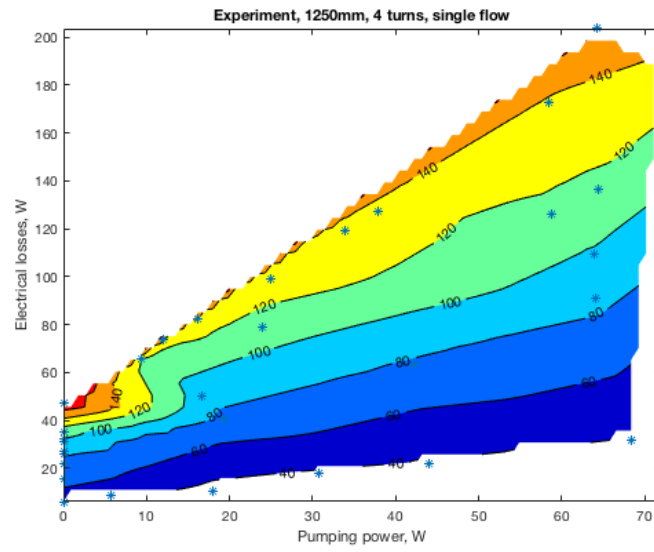Figure 69: Experiment results showing current density versus inlet pressure

Figure 70: Experiment results showing heat load versus pump power

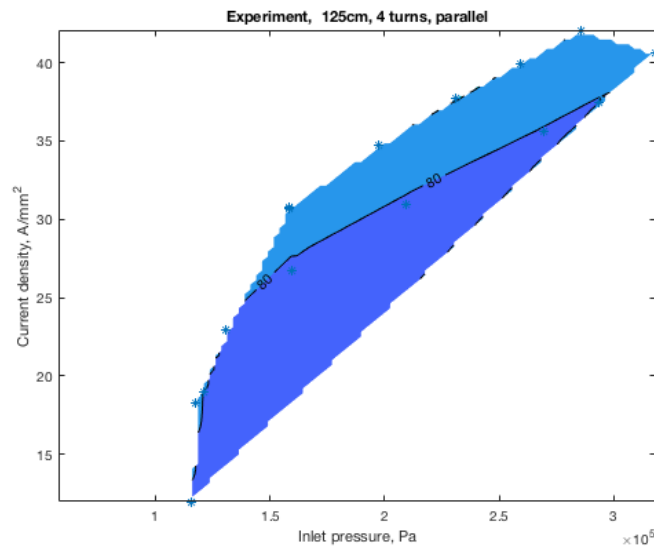**1250mm hollow conductor 4 turns parallel flow**

Figure 71: Experiment results showing current density versus inlet pressure
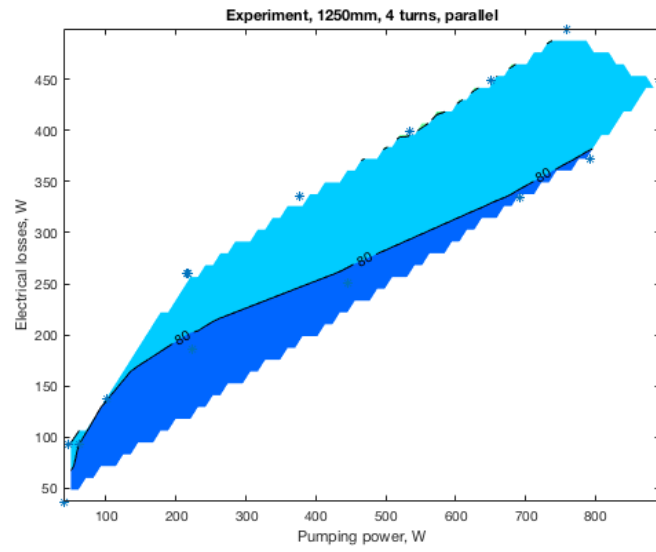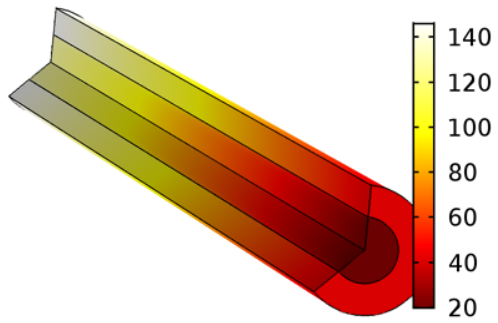
Figure 72: Experiment results showing heat load versus pump power

14.2   Comsol reports

200mm Copper Tube

Author

Michael Gabassi

Report date

Apr 5, 2018 11:37:18 AM

Contents

1 Global Definitions

Date	Mar 27, 2018 9:22:18 PM

1.1 PARAMETERS 1

PARAMETERS

Name	Expression	Value	Description
H	0.2[m]	0.2 m	Lenth of pipe
D	3.9088[mm]	0.0039088 m	Outer diameter
d	2[mm]	0.002 m	Inner diameter
Tin	20[degC]	293.15 K	Inlet temperature
A	pi*(D^2 - d^2)/4	8.8583E−6 m^2	Copper cross-sectional area
u_init	100[m/s]	100 m/s	initial guess of velocity
p_in	1[bar]	1E5 Pa	inlet pressure, gage
T_init	100[degC]	373.15 K	initial temperature
Q_in	100[W]	100 W	Heat load
q_in	Q_in/(A*H)	5.6444E7 W/m^3	distributed heat load

2   Component 1

2.1   DEFINITIONS

2.1.1   Coordinate Systems

Boundary System 1

Coordinate system type	Boundary system
Tag	sys1

2.2   GEOMETRY 1
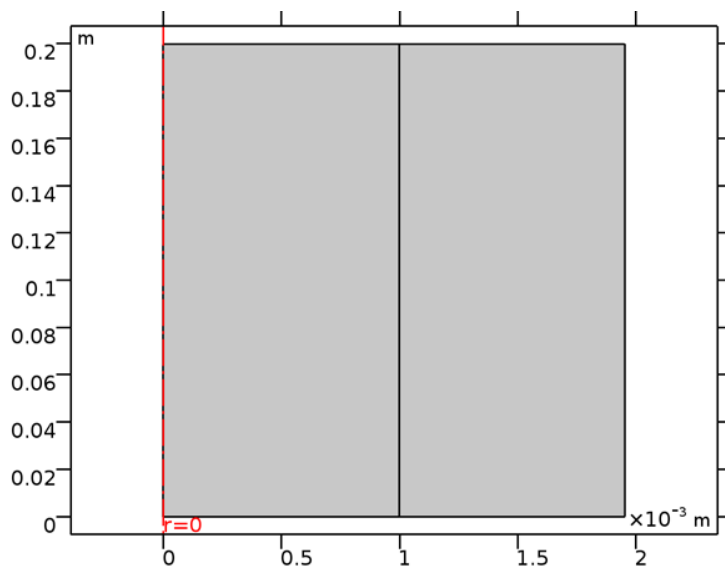
Geometry 1

UNITS

Length unit	m
Angular unit	deg

2.3 MATERIALS

2.3.1 Copper
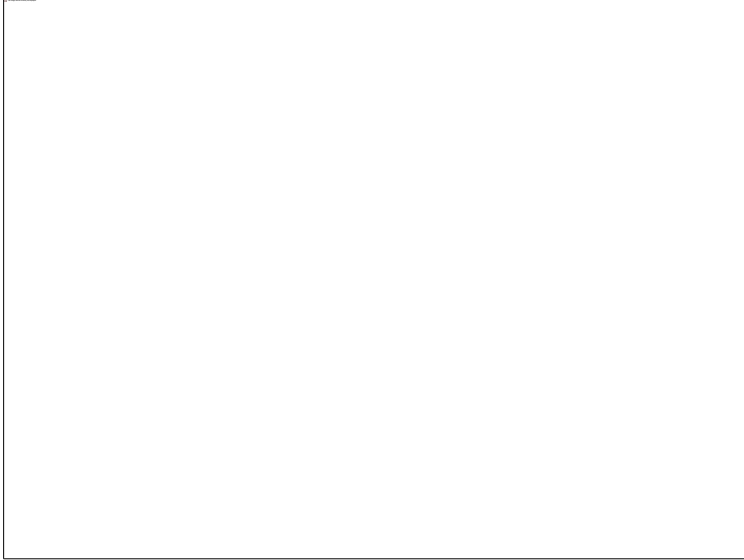
Copper

Geometric entity level	Domain
Selection	Domain 2

2.3.2 Copper
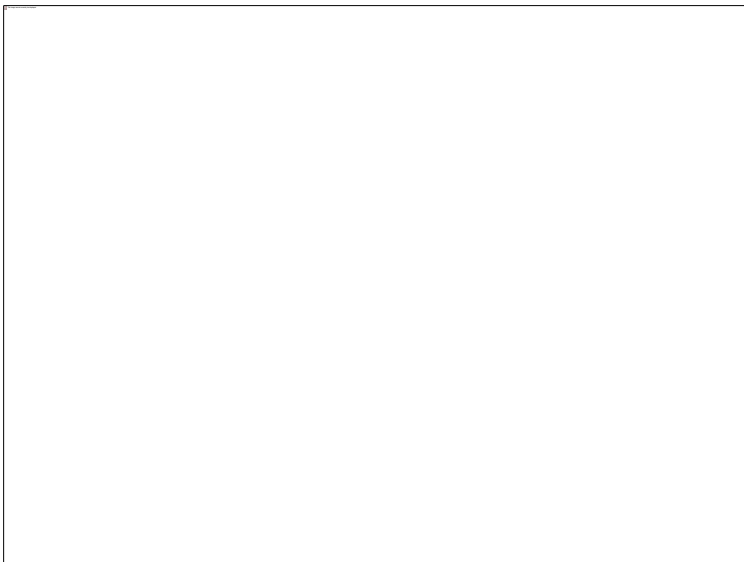
Copper

Geometric entity level	Domain
Selection	Domain 2

2.3.3 Copper
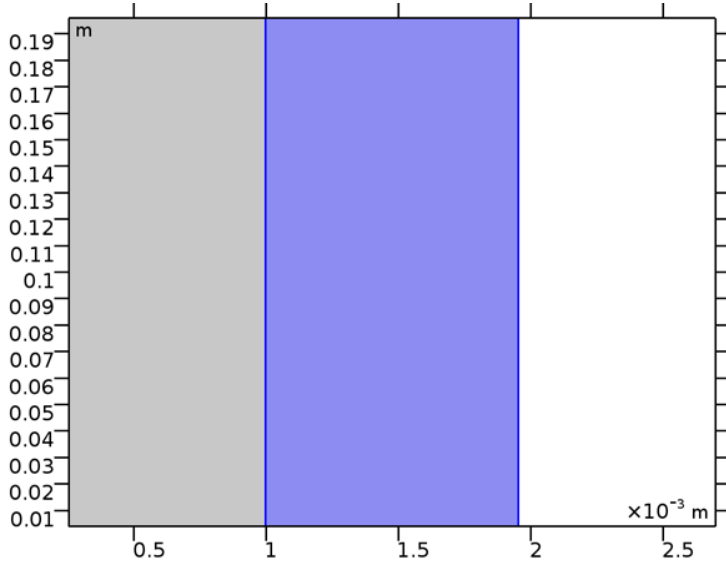
Copper

Geometric entity level	Domain
Selection	Domain 2

2.4 HEAT TRANSFER
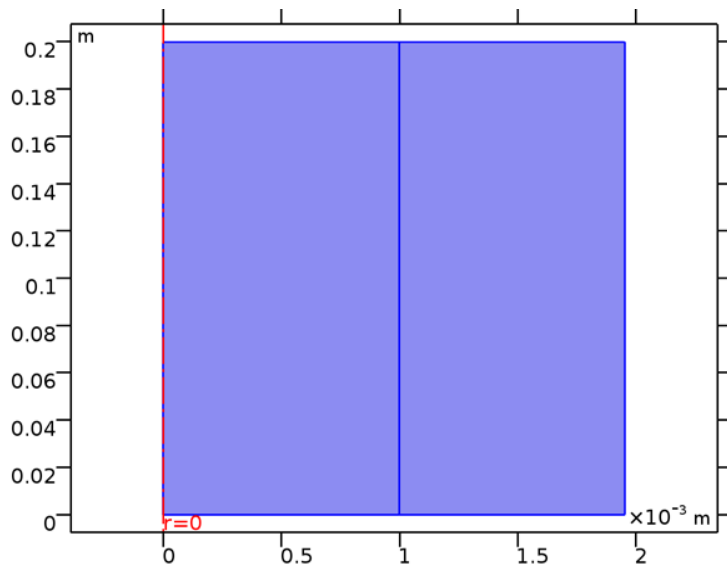
Heat Transfer

FEATURES

Solid 1
Fluid 1
Initial Values 1
Axial Symmetry 1
Thermal Insulation 1
Heat Source 1
Temperature 2
Heat Flux 1

2.4.1 Solid 1
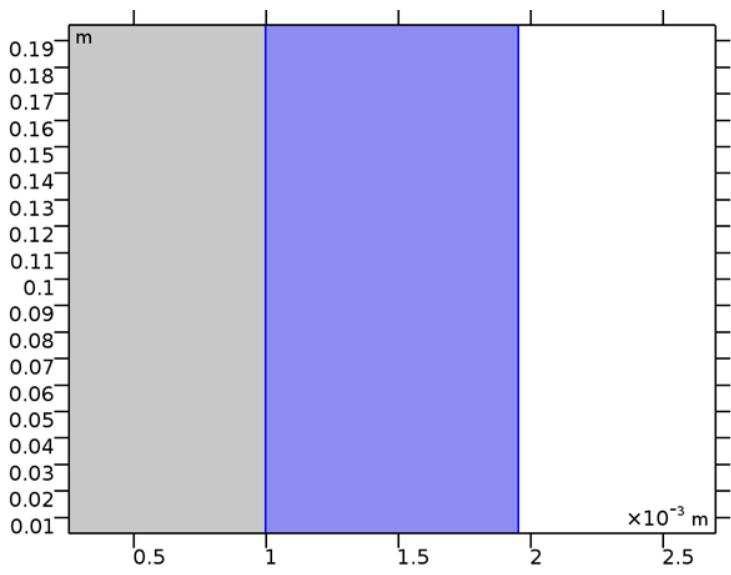
Solid 1

2.4.2 Fluid 1
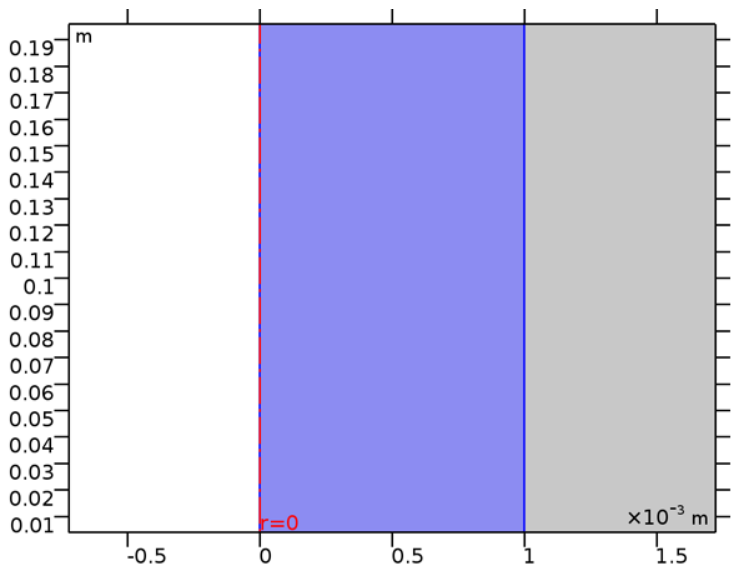
Fluid 1

2.4.3 Heat Source 1
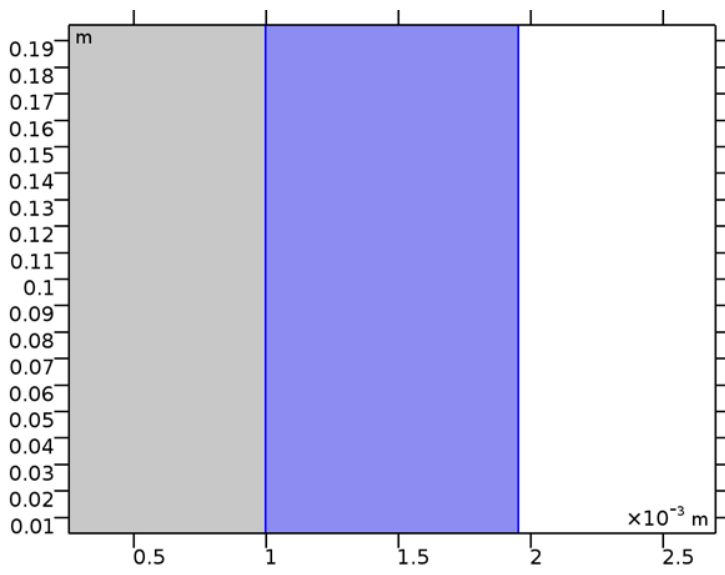
Heat Source 1

SETTINGS

Description	Value
Heat source	General source
Heat source	User defined
Heat source	q_in

2.4.4 Temperature 2
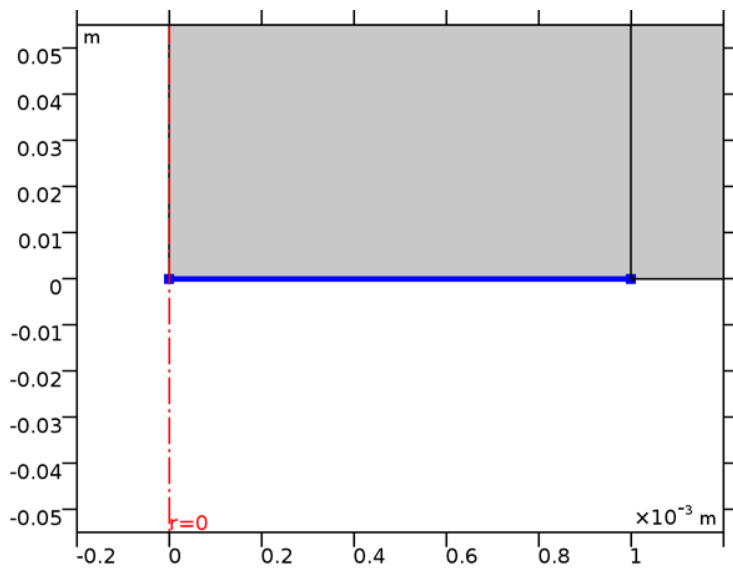
Temperature 2

Description	Value
	Classic constraints
Apply reaction terms on	All physics (symmetric)
Constraint method	Elemental
Use weak constraints	Off
Temperature	User defined
Temperature	Tin

2.4.5 Heat Flux 1
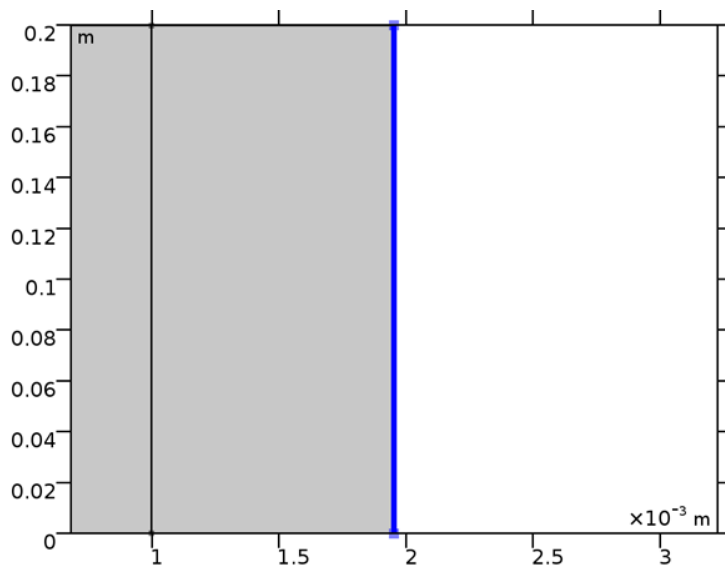
Heat Flux 1

SETTINGS

Description	Value
Heat flux	Convective heat flux
Heat transfer coefficient	User defined
Heat transfer coefficient	15
External temperature	User defined
External temperature	293.15[K]

2.5 MULTIPHYSICS

2.5.1 Nonisothermal Flow 1
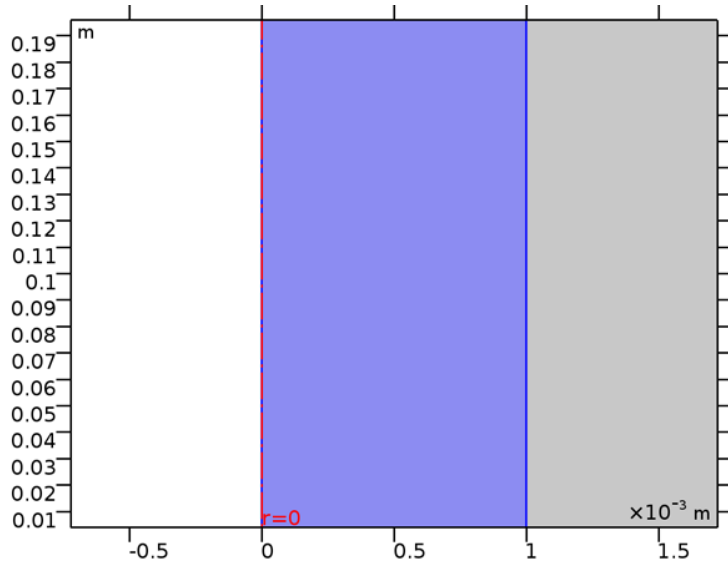
Nonisothermal Flow 1

3 Study 1

COMPUTATION INFORMATION

Computation time	2 h 21 min 11 s
CPU	AMD FX(tm)-6300 Six-Core Processor, 3 cores
Operating system	Windows 7

3.1 PARAMETRIC SWEEP

Parameter name	Parameter value list	Parameter unit
Q_in	10,10,10,10,10,32.5,32.5,32.5,32.5,32.5,55,55,55,55,55,77.5,77.5,77.5,77.5,77.5,100,100,100,100,100,100,125,125,125,150,150,150,140,160,200	W
p_in	0.51,1.285,2.06,2.835,3.61,0.51,1.285,2.06,2.835,3.61,0.51,1.285,2.06,2.835,3.61,0.51,1.285,2.06,2.835,3.61,0.51,1.285,2.06,2.51,3.06,3.61,2.51,3.06,3.61,2.51,3.06,3.61,2,3,3	bar

STUDY SETTINGS

Description	Value
Sweep type	Specified combinations
Parameter name	{Q_in, p_in}
Parameter value list	{10, 10, 10, 10, 10, 32.5, 32.5, 32.5, 32.5, 32.5, 55, 55, 55, 55, 55, 77.5, 77.5, 77.5, 77.5, 77.5, 100, 100, 100, 100, 100, 100, 125, 125, 125, 150, 150, 150, 140, 160, 200, 0.51, 1.285, 2.06, 2.835, 3.61, 0.51, 1.285, 2.06, 2.835, 3.61, 0.51, 1.285, 2.06, 2.835, 3.61, 0.51, 1.285, 2.06, 2.835, 3.61, 0.51, 1.285, 2.06, 2.51, 3.06, 3.61, 2.51, 3.06, 3.61, 2.51, 3.06, 3.61, 2, 3, 3}
Unit	{W, bar}

3.2 WALL DISTANCE INITIALIZATION

STUDY SETTINGS

Description	Value
Include geometric nonlinearity	Off

PHYSICS AND VARIABLES SELECTION

Physics interface	Discretization
Heat Transfer (ht)	physics
Turbulent Flow, Algebraic yPlus (spf)	physics

MESH SELECTION

Geometry	Mesh
Geometry 1 (geom1)	mesh1

3.3 STATIONARY

Description	Value
Include geometric nonlinearity	Off

PHYSICS AND VARIABLES SELECTION

Physics interface	Discretization
Heat Transfer (ht)	physics
Turbulent Flow, Algebraic yPlus (spf)	physics

MESH SELECTION

Geometry	Mesh
Geometry 1 (geom1)	mesh1

4 Results

4.1 TABLES

4.1.1 Copper Max. Temp

Surface Maximum 1 (T)

COPPER MAX. TEMP

Q_in (W)	p_in (bar)	Temperature (degC)
10.000	0.51000	45.517
10.000	1.2850	36.223
10.000	2.0600	31.949
10.000	2.8350	29.287
10.000	3.6100	27.714
32.500	0.51000	106.70
32.500	1.2850	74.391
32.500	2.0600	60.467
32.500	2.8350	50.965
32.500	3.6100	45.567
55.000	0.51000	173.86
55.000	1.2850	114.96
55.000	2.0600	90.678
55.000	2.8350	73.860
55.000	3.6100	64.144
77.500	0.51000	248.96
77.500	1.2850	157.91
77.500	2.0600	122.28
77.500	2.8350	98.340
77.500	3.6100	83.476
100.00	0.51000	331.32
100.00	1.2850	203.19
100.00	2.0600	155.21
100.00	2.5100	137.09
100.00	3.0600	117.18
100.00	3.6100	103.64
125.00	2.5100	170.49
125.00	3.0600	146.22

Q_in (W)	p_in (bar)	Temperature (degC)
125.00	3.6100	127.11
150.00	2.5100	205.06
150.00	3.0600	176.78
150.00	3.6100	151.95
140.00	2.0000	221.24
160.00	3.0000	192.41
200.00	3.0000	244.22

4.1.2 Copper Avg. Temp

Surface Average 1 (T)

COPPER AVG. TEMP

Q_in (W)	p_in (bar)	Temperature (degC)
10.000	0.51000	36.100
10.000	1.2850	29.959
10.000	2.0600	27.276
10.000	2.8350	25.643
10.000	3.6100	24.684
32.500	0.51000	74.865
32.500	1.2850	53.408
32.500	2.0600	44.670
32.500	2.8350	38.817
32.500	3.6100	35.527
55.000	0.51000	117.71
55.000	1.2850	78.358
55.000	2.0600	63.119
55.000	2.8350	52.729
55.000	3.6100	46.814
77.500	0.51000	166.10
77.500	1.2850	104.84
77.500	2.0600	82.432
77.500	2.8350	67.608
77.500	3.6100	58.558
100.00	0.51000	219.97
100.00	1.2850	132.82
100.00	2.0600	102.56

Q_in (W)	p_in (bar)	Temperature (degC)
100.00	2.5100	91.335
100.00	3.0600	79.051
100.00	3.6100	70.818
125.00	2.5100	111.74
125.00	3.0600	96.731
125.00	3.6100	85.075
150.00	2.5100	132.87
150.00	3.0600	115.37
150.00	3.6100	100.17
140.00	2.0000	143.00
160.00	3.0000	124.95
200.00	3.0000	156.59

4.1.3 Avg. Flow Velocity

Surface Average 2 (spf.U)

AVG. FLOW VELOCITY

Q_in (W)	p_in (bar)	Velocity magnitude (m/s)
10.000	0.51000	72.126
10.000	1.2850	98.188
10.000	2.0600	111.00
10.000	2.8350	118.41
10.000	3.6100	120.73
32.500	0.51000	74.172
32.500	1.2850	99.650
32.500	2.0600	110.20
32.500	2.8350	118.36
32.500	3.6100	120.88
55.000	0.51000	75.986
55.000	1.2850	101.25
55.000	2.0600	110.64
55.000	2.8350	118.20
55.000	3.6100	121.03
77.500	0.51000	77.308
77.500	1.2850	103.06
77.500	2.0600	111.70

Q_in (W)	p_in (bar)	Velocity magnitude (m/s)
77.500	2.8350	117.71
77.500	3.6100	121.22
100.00	0.51000	78.860
100.00	1.2850	105.08
100.00	2.0600	113.07
100.00	2.5100	115.08
100.00	3.0600	118.83
100.00	3.6100	121.39
125.00	2.5100	116.18
125.00	3.0600	118.20
125.00	3.6100	121.56
150.00	2.5100	117.62
150.00	3.0600	118.34
150.00	3.6100	121.59
140.00	2.0000	115.53
160.00	3.0000	118.49
200.00	3.0000	120.38

4.2   PLOT GROUPS

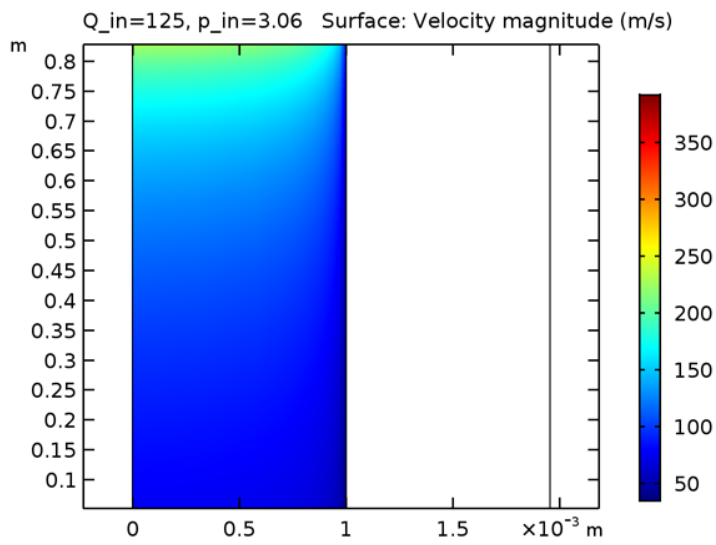### 4.2.1 Temperature, 3D (ht)

Q_in=125, p_in=3.06 Surface: Temperature (degC)

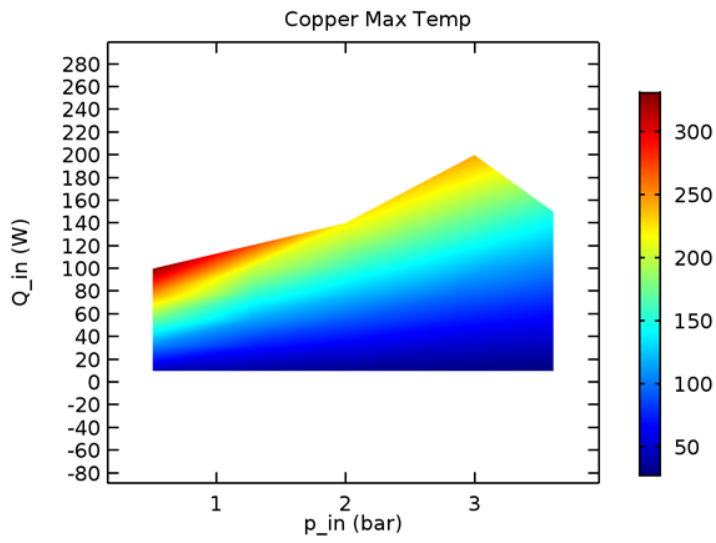### 4.2.2 Isothermal Contours (ht)
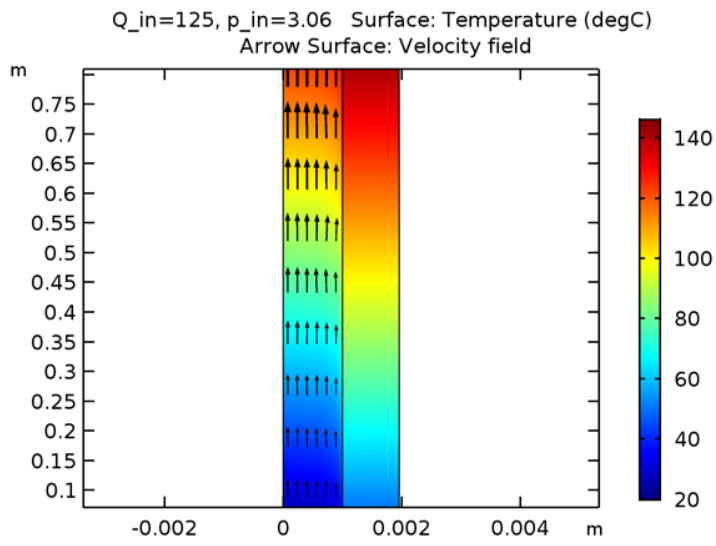
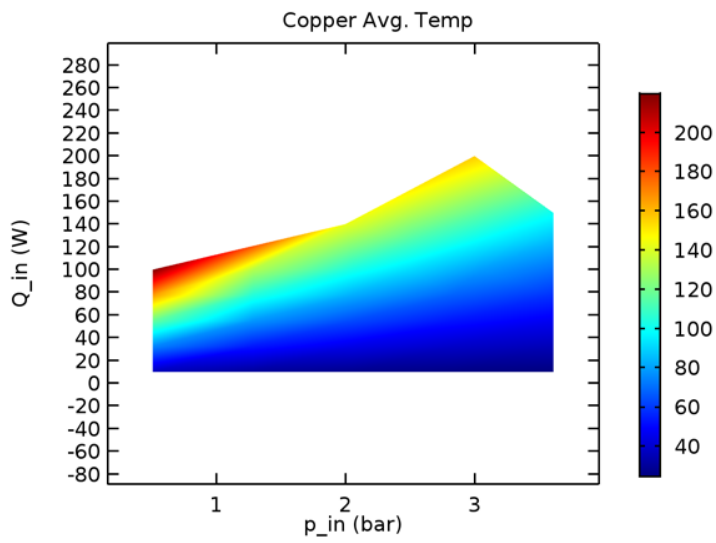*Temperature distribution with flow vectors*

4.2.3 Velocity (spf)

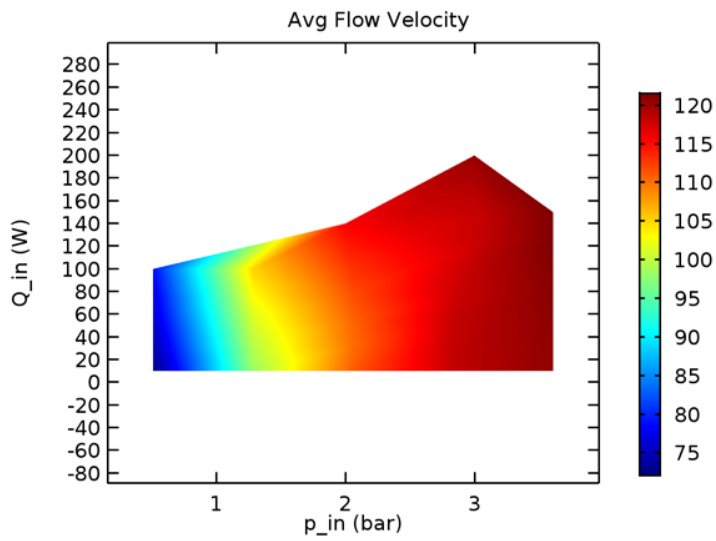*Q_in=125, p_in=3.06 Surface: Velocity magnitude (m/s)*

4.2.4 2D Plot Group 21

Copper Max Temp

4.2.5 2D Plot Group 22
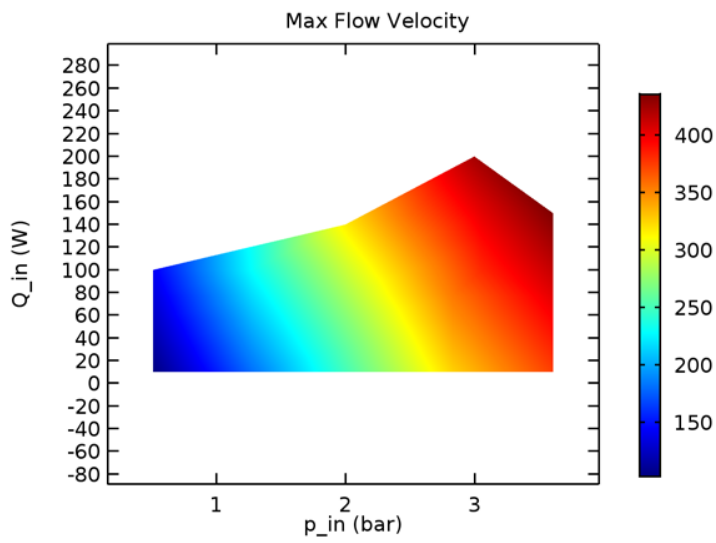

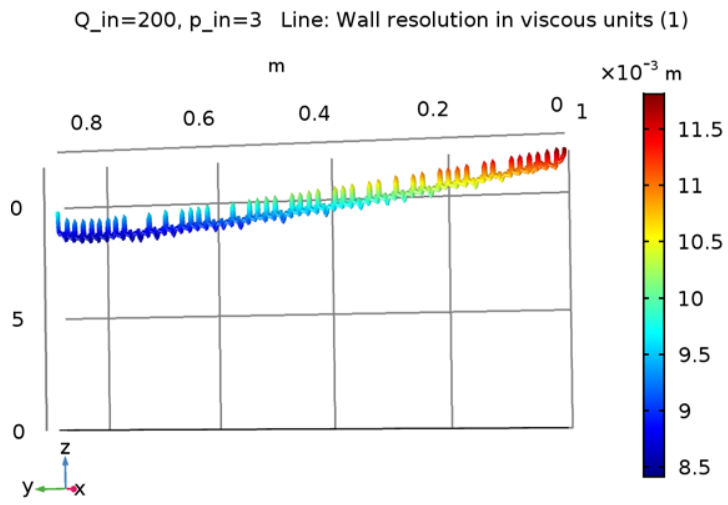Copper Avg. Temp

4.2.6 2D Plot Group 23

Avg Flow Velocity

4.2.7 2D Plot Group 24

Max Flow Velocity

4.2.8   Wall Resolution (spf)

Q_in=200, p_in=3 Line: Wall resolution in viscous units (1)

1250mm hollow conductor

Author

Michael Gabassi

Report date

Apr 6, 2018 5:27:29 PM

1 Results

1.1 TABLES

1.1.1 Copper temperatures

Copper maximum temperature (T)

COPPER TEMPERATURES

Q_in (W)	p_in (bar)	Max Temp (degC)	Avg Temp (degC)	Pump power (W)
40.214	0.98650	103.33	71.491	15.668
63.254	2.0084	105.80	71.281	37.530
90.849	3.0003	112.83	74.897	59.718
109.55	2.9999	134.22	87.587	58.193
136.55	3.0171	165.93	106.44	56.407
203.57	3.0110	256.07	160.23	50.621
50.195	0.87242	131.81	89.670	13.135
79.162	1.1923	177.23	116.64	18.208
125.92	2.7601	163.40	105.11	51.037
172.81	2.7471	230.48	145.22	46.649
188.87	3.3679	213.67	134.58	60.611
127.22	1.8166	228.58	146.12	28.118
118.97	1.6359	226.81	145.61	25.012
99.295	1.2368	218.33	141.96	18.312
82.313	0.85261	213.76	141.61	11.835
73.494	0.66770	209.96	141.11	8.7971
65.511	0.54511	201.13	137.06	6.8626
10.747	0.92740	41.926	33.539	15.566
17.836	1.4975	47.848	36.789	28.274
21.999	2.0866	47.135	36.156	42.987
31.849	3.2053	49.104	37.151	69.607

1.1.2 Fluid Velocities

Line Average 2 (spf.U)

FLUID VELOCITIES

Q_in (W)	p_in (bar)	Max. velocity (m/s)	Avg. Velocity (m/s)	spf.U*Afluid*p_in (W)
40.214	0.98650	138.73	83.859	15.668

Q_in (W)	p_in (bar)	Max. velocity (m/s)	Avg. Velocity (m/s)	spf.U*Afluid*p_in (W)
63.254	2.0084	241.58	105.80	37.530
90.849	3.0003	337.06	114.91	59.718
109.55	2.9999	345.80	115.41	58.193
136.55	3.0171	359.78	116.23	56.407
203.57	3.0110	389.46	117.93	50.621
50.195	0.87242	133.30	81.669	13.135
79.162	1.1923	174.54	92.262	18.208
125.92	2.7601	334.85	114.76	51.037
172.81	2.7471	354.09	115.54	46.649
188.87	3.3679	408.23	118.68	60.611
127.22	1.8166	250.33	105.08	28.118
118.97	1.6359	231.11	102.60	25.012
99.295	1.2368	187.83	95.128	18.312
82.313	0.85261	145.43	84.582	11.835
73.494	0.66770	123.65	77.481	8.7971
65.511	0.54511	107.75	71.426	6.8626
10.747	0.92740	120.07	79.627	15.566
17.836	1.4975	174.41	95.339	28.274
21.999	2.0866	231.33	106.76	42.987
31.849	3.2053	323.61	114.17	69.607

1.2 PLOT GROUPS

1.2.1 Fluid center velocity
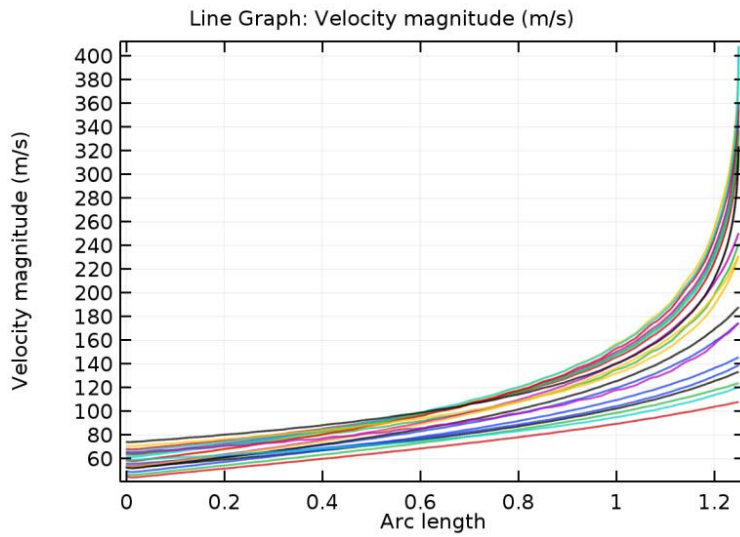
Line Graph: Velocity magnitude (m/s)

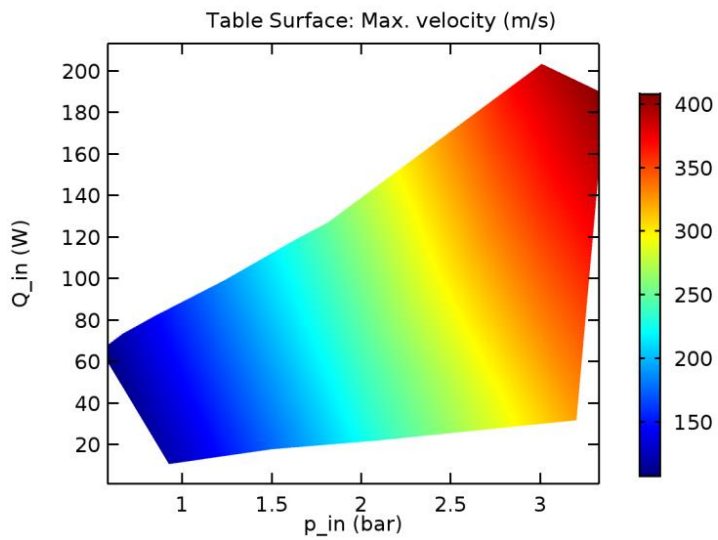### 1.2.2 max velocity

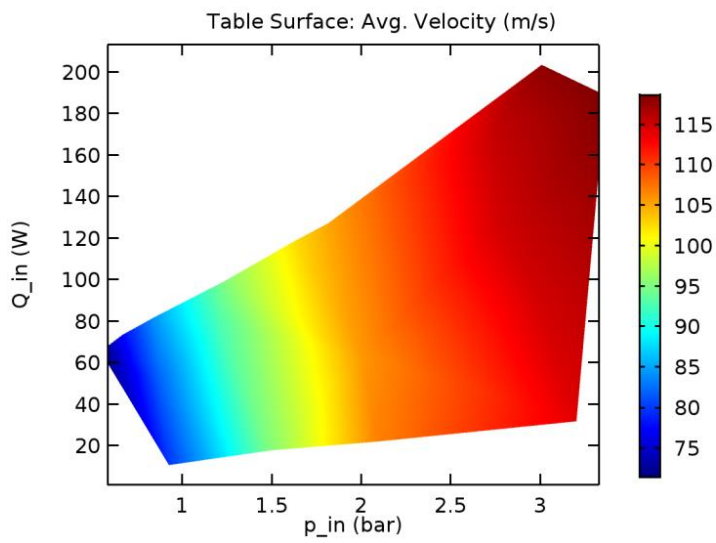*Table Surface: Max. velocity (m/s)*

1.2.3   avg velocity

Table Surface: Avg. Velocity (m/s)

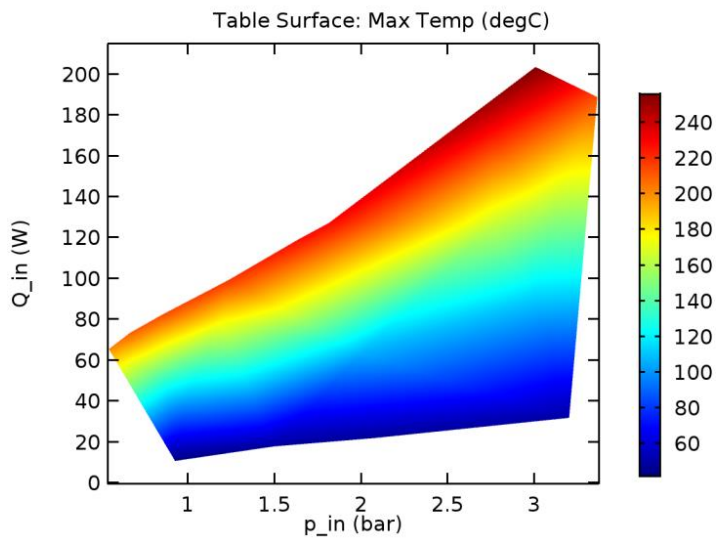### 1.2.4   Max temperature

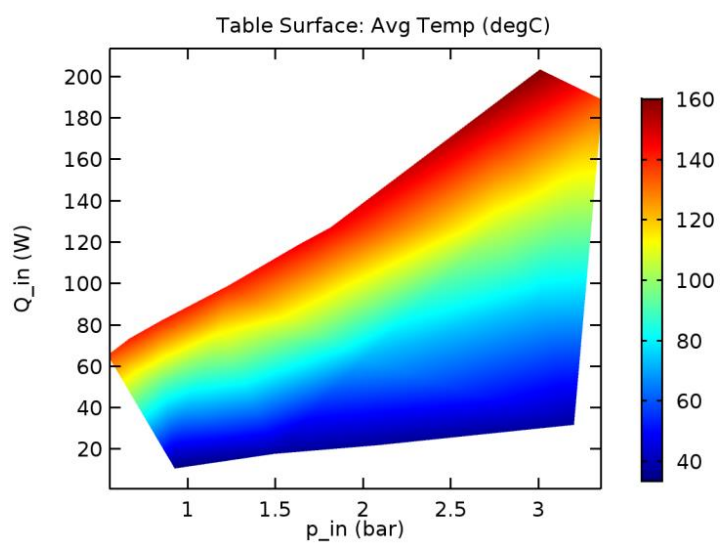*Table Surface: Max Temp (degC)*
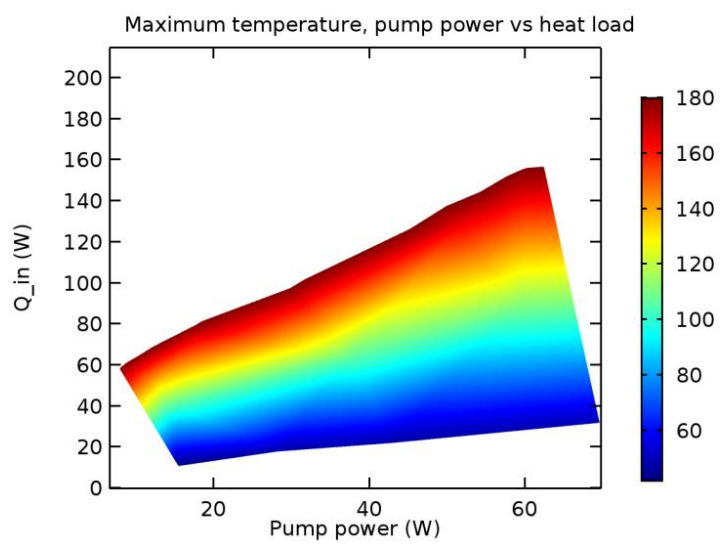
1.2.5 avg temperature

Table Surface: Avg Temp (degC)

1.2.6 avg temperature 1

Maximum temperature, pump power vs heat load

References

[1] C. M. Laffoon. "Internally cooled generator coils increase ratings by one-half". In: *Electrical Engineering* 70.11 (1951), pp. 1013–1015. DOI: 10.1109/ee.1951.6436938.

[2] B. Sundén. *Introduction to Heat Transfer*. 1st ed. Department of Energy Sciences, Lund University, 2008.

[3] J. D. Anderson. *Fundamentals of aerodynamics*. 5th ed. McGraw-Hill, 2011. ISBN: 0073398101.

[4] F. M. White. *Fluid Mechanics*. 7th ed. Mc Graw Hill, 2011. ISBN: 9780071311212.

[5] W. Frei. 2017. URL: https://www.comsol.com/blogs/which-turbulence-model-should-choose-cfd-application/ (visited on 02/02/2018).

[6] *ELFA DISTRELEC*. URL: https://www.elfa.se/en/pressure-sensor-16-bar-10-gems-3500s0016a05e000/p/30073784?q=gems+3500&page=8&origPos=8&origPageSize=25&simi=97.0 (visited on 02/02/2018).

[7] *Keysight Technologies*. URL: https://www.keysight.com/en/pd-1756491-pn-34972A/lxi-data-acquisition-data-logger-switch-unit?cc=SE&lc=swe (visited on 02/02/2018).

[8] *VP Instruments*. URL: http://www.innovativeinstruments.com/ii/wp-content/uploads/2014/01/vp-Manuale-usoIstruzioni-VP-flow-Mate (visited on 02/02/2018).